NASA Contractor Report 159049

Fatigue Life Prediction of Bonded Primary Joints

J. F. Knauss

VOUGHT CORPORATION ADVANCED TECHNOLOGY CENTER
P. O. BOX 226144
DALLAS, TEXAS 75266

CONTRACT NAS1-15188
SEPTEMBER 1979

National Aeronautics and
Space Administration

Langley Research Center
Hampton, Virginia 23665

FATIGUE LIFE PREDICTION OF BONDED PRIMARY JOINTS

FINAL REPORT

Period Covering
1 February 1978 to 15 March 1979

ATC Report No. R-92100/9CRL-17

September 1979

Prepared for

STRUCTURAL INTEGRITY BRANCH
NASA-Langley
Hampton, Va. 23665

Prepared by

J. F. Knauss

VOUGHT CORPORATION ADVANCED TECHNOLOGY CENTER
P. O. Box 226144
Dallas, Texas 75265

FOREWORD

The study reported in this program entitled "Fatigue Life Prediction of Bonded Joints"* was conducted by Vought Corporation Advanced Technology Center and was sponsored by the National Aeronautics and Space Administration through Langley Research Center under Contract Number NAS1-15188.

Dr. J. H. Crews, Jr. was the NASA Technical Monitor and Dr. W. J. Renton was the Vought Program Manager. Other key personnel were Mr. J. F. Knauss, Principal Investigator, Dr. D. H. Petersen, Technical Coordinator and Dr. R. A. Schapery, Technical Consultant. Acoustic emission development was performed by Mr. C. L. Shank and mechanical testing by Mr. J. H. Thomas. Dr. Schapery is responsible for the analytical development of Appendices A and B.

This study was conducted from February 1978 through March 1979.

* The contract research effort which has led to the results in this report was financially supported by the Structures Laboratory, USARTL (AVRADCOM).

TABLE OF CONTENTS

	Page Number
FOREWORD	i
LIST OF SYMBOLS	iii
1.0 INTRODUCTION	1
2.0 BONDING PROCEDURES	3
2.1 Adhesive Selection	3
2.2 Surface Preparation	6
2.3 Specimen Fabrication	7
2.3.1 Contoured Double Cantilever Beam Specimen Bonding	7
2.3.2 Butt and Scarf Joint Bonding	7
2.4 Non-Destructive Inspection	9
3.0 ADHESIVE CHARACTERIZATION	13
3.1 Bulk Adhesive Tests	13
3.2 Double Cantilever Beam Specimen Tests	13
4.0 MECHANICAL TESTING	23
4.1 Test Specimen Configuration	23
4.2 Failure Surface Observations	26
4.3 Analysis of Fatigue Data	27
5.0 ACOUSTIC EMISSION	36
5.1 General Background	36
5.2 Experimental Approach	37
5.3 Experimental Observations	41
6.0 DISCUSSION AND CONCLUSIONS	54
7.0 SUMMARY	56
REFERENCES	57
APPENDIX A	A-1
APPENDIX B	B-1

LIST OF SYMBOLS

a	crack length
a_o	initial crack length
A/E	acoustic emission
b	shape parameter (exponent in probability function)
C	time dependence of crack growth coefficient
c	ordinate intercept of Rate-K relationship and coefficient of power law crack growth equation
c_1	reflects small scale local adhesive material properties
c_2	reflects large scale "effective" adhesive material properties
dB	decibels
E	Young's modulus
F_i	statistically distributed exponent representing crack growth of ith specimen
I_f	critical value of I_N at which crack growth becomes unstable
I_N	integration of the crack growth equation
I_N/I_f	damage ratio
K	stress intensity factor
ΔL_i	load amplitudes in fatigue loading
m	CDCB specimen contour parameter
N	number of cycles in fatigue loading or force measurement unit (Newton)
N_f	number of cycles to failure (mean fatigue lifetime)
$\tilde{N}$	"reduced life" parameter
p	defined for convenience as $(q/2)-1$
P_f	failure probability function
P_F	failure probability function relating to F

LIST OF SYMBOLS (CONT'D.)

q	slope of Rate-K relationship and exponent in power law crack growth equation
R	stress ratio (minimum stress/maximum stress)
t_f	global failure time
t_f'	local failure time
T_R	reference temperature
η	frequency
ν	Poisson's ratio
σ_n	bondline normal stress in analysis
σ_s, σ_z	bondline inplane stresses in analysis
σ_{T_u}	ultimate tensile strength

1.0 INTRODUCTION

The wide usage of advanced composite materials in future aerospace systems is projected to become a reality over the next ten years. Inherent complications exist in the mechanical fastening of composites to primary structure due to their brittle nature and relatively low bearing strength. Adhesive attachment relieves the characteristic stress concentrations associated with mechanical fastening, but little is known about the behavior of adhesively bonded composites under long-term fatigue environments.

This research program sought to validate a proposed fatigue life prediction methodology through the use of aluminum butt and scarf joint and graphite/epoxy butt joint specimens in a constant amplitude fatigue environment. The structural properties of the HYSOL 9313 adhesive system were obtained by mechanical test of molded neat adhesive specimens. Aluminum contoured double cantilever beam (CDCB) specimens were used to generate crack velocity versus stress intensity factor data.

The specific objectives of this research effort were:

- To ascertain the feasibility of predicting fatigue failure of an adhesive in a primary bonded composite structure by incorporating linear elastic crack growth behavior in the life prediction methodology.
- To ascertain if acoustic emission and/or compliance measurement techniques can be used to detect flaw initiation and propagation in the adhesive of the bonded structure.

This report covers a 13 month exploratory development program of the proposed research. All experimental measurements were made in customary (English) units and converted to the International System of Units (S.I.) for this report.

2.0 BONDING PROCEDURES

2.1 Adhesive Selection

Adhesive selection criteria were based on several basic requirements as outlined in Table 2-1. Not only should the selected adhesive fulfill strength requirements but it was to bond equally well to the different adherends planned for use in the program (lucite, aluminum, and graphite/epoxy composite). These requirements alone set the limits to a very narrow range of adhesive types. Because of the low temperature resistance of lucite, (125° - 140°F (325-333K)) additional consideration was cure temperature, which indicated that a low temperature, two-part catalyst cure epoxy was desirable. Other important criteria were transparency, viscosity control, somewhat brittle characteristics, good literature characterization, and ease of handling. The adhesives which met most of the requirements and were under consideration are listed in Table 2-2.

Very little information was available in the literature on adhesives with such broad applicability as was desired in this program. This broad range of adherend types greatly restricted the range of adhesive physical and chemical characteristics and eliminated many other systems which were attractive for specific bonding applications. Outside of these considerations but also of utmost importance to this program were, of course, the tension and fatigue properties of each individual adhesives.

Fabrication of bulk adhesive material suitable for tension and fatigue testing was carried out on the four most likely candidate adhesives. These four adhesives which best suited all selection criterion consisted of the Shell Epon 828 resin with three different curing agents [Diethylaminopropylamine (DTA), Shell V-25 curing agent and V-140 curing agent] and Hysol 9313 adhesive with catalyst. In order to assure a test piece of sufficient size to machine into several dog-bone shapes, a 10.2 x 12.7 cm (4 x 5 inch) mold was utilized. All adhesives were formulated with their curing agents and were then vacuum degassed and centrifuged to eliminate bubbles. Bulk cure of the specimens was according to manufacturer's recommended procedure. Removal from the mold and machining required delicate handling due to the brittle nature of some of the materials. These bulk adhesive specimens were then tested in tension and fatigue as reported in Section 3.1 of this report.

TABLE 2-1

ADHESIVE SELECTION CRITERIA

1. Must be capable of bonding together lucite elements, aluminum elements, and graphite/epoxy composite elements.

2. Low temperature cure

3. Good transparency

4. Must have a somewhat brittle character

5. Viscosity control must be possible without the use of Cab-O-Sil or other fillers to assure a bondline of neat adhesive material.

6. Preferably no more than a two-part formulation for ease of fabrication.

7. Formulation tailoring for cure times and viscosity to suit the specific requirements of the program.

8. Should require no special handling requirements.

9. Should be well characterized in literature.

TABLE 2-2. ADHESIVE SELECTION CRITERIA

ADHESIVE	REMARKS	Applicable To Three Adherends	Low Cure Temperature	Transparent	Brittle Character	Meets Military Specification	Viscosity Control	No More Than 2 Part Formula	No Special Handling	Well Characterized In Literature	Catalyst Tailoring	Remarks
American Cyanimid BR-92	Toughened ~5000 PSI	✓				✓	✓	✓	✓	✓		Not Transparent
Shell Epon 828 (Curing Agent A)	Catalyst Not Available From Shell	✓	✓ R.T. + 100°F	✓	✓			✓	✓		✓	
Furane Epohond 121	~2500 PSI	✓	✓ R.T. (4-7 Days)	✓			✓	✓				
Furane Epibond 101		✓	✓				✓	✓				Transparency A Problem
Shell Epon 828 (V-25 Catalyst)	Curing Agent Ordered Polyimide	✓	✓ R.T. + 80°F	✓	✓	✓	✓	✓	✓	✓	✓	
Shell Epon 828 (DTA Catalyst)	DTA On Hand	✓	✓	✓	✓	✓	✓	✓	✓	✓	✓	
Hysol 956	Has Some Cab-O-Sil (Can order Some Without)	✓		✓	✓	✓	✓	✓	✓	✓	✓	
Hysol 9313	Toughened	✓	✓	Slightly Cloudy	Toughened	✓	✓	✓	✓	✓	✓	
Shell Epon 828 (V-40 Cure)	Catalyst On Hand	✓	✓	✓	✓	✓	✓	✓	✓	✓	✓	

Utilization of the HYSOL 9313 adhesive system finally chosen from these tests required handling and lay-up procedures specifically designed to accomodate test specimen configurations selected for this program. Surface preparation and jig configuration for the contoured double cantilever beam (CDCB) and the butt and scarf joint test specimens are discussed in the following section.

2.2 Surface Preparation

A standard procedure for obtaining uniformity in the bonding surfaces for adhesive joints was followed throughout this program. Initial procedures for bonding the lucite adherends proved inadequate and therefore a more detailed surface pattern (tooth) was introduced for the lucite as well as the graphite/epoxy adherends.The procedure for the surface preparation for all aluminum surfaces whether for the cantilever beams or for the butt/scarf specimen was the phosphoric anodize system developed by the Boeing Company. [Process Specification No. BAC5555] All aluminum adherends were anodized in preparation for bonding not more than 24 hours prior to adhesive lay-up, and standard controls to eliminate contamination, e.g., measures such as Kraft paper wrapping and cotton glove handling, were incorporated in order to prevent introduction of substances detrimental to adhesion prior to bonding. All aluminum adherends were carried through the Vought Bond Clean and Phosphoric Acid Anodize facilities and inspected prior to bonding. Inspection consisted of close examination of the bonding surface to insure against rack carrier damage during anodizing and observation of the "interference" colors with a polarizing lens, verifying the presence of the phosphoric anodic coating. These control measures are standard bonding requirements for structural adhesives.

The flat machined surfaces of the graphite/epoxy adherends were prepared for bonding following cleaning and surface texture application which conformed to recommendations of the adhesive manufacturer. A cross-hatch pattern was applied to the machined surfaces with the use of a non-wettable sandpaper and the surface was thoroughly cleaned and dried using three separate wash-wipes of methyl-ethyl-ketone (reagent grade) just prior to bonding. Contamination-prevention procedures followed for the graphite/epoxy adherends were similar to those used for the aluminum adherends.

2.3 Specimen Fabrication

2.3.1 Contoured Double Cantilever Beam (CDCB) Specimen Bonding

The bonding procedure followed in preparing the CDCB test specimen required construction of a special jig, Figure 2-1. This figure shows the damming well running the entire length of the apparatus along the bondline. Mold release agent was applied to the surface before laying down full length strips of the tacky tape dam material. 0.64 cm (0.25 inch) wide teflon tape was centered along the length of the tacky tape to become the material which actually made contact with the bondline. Steel shims were placed at each end of the cantilever beam specimen for thickness control, and acted as adhesive dams in these areas. Sprayed with mold release, these shims were easily removed after post-cure. The shim at the loaded end of the specimen was contoured in order to provide a pointed end to the bondline and, thus, enhance crack initiation. Damming material plugs in the holes at each end kept the shims in place during adhesive application and also prevented accidental filling of the loading holes with excess adhesive.

Ten minutes prior to use, the adhesive/catalyst system was mixed and then applied following manufacturer's recommended procedure for HYSOL 9313. The cure cycle required a minimum of 6 hours at room temperature with a minimum post-cure of 24 hours at 130°F (327.6K). Cure times were adjusted for schedules and consistency to a six day post cure.

Alignment pins at each end of the jig ensured proper adherend profile and maintained bondline thickness.

2.3.2 Butt and Scarf Joint Bonding

The bonding procedure followed in preparing the test joints for the three different types of adherends was similar in all cases. Although surface preparation for the different adherends varied from one material to the others, the same jig was used for all test pieces. The damming well Figure 2-2 ran along the bondline and extended to either side of the bond. A mold release agent was applied to the surface before laying down full length strips of the tacky tape dam material. A 0.635 cm (0.25 inch) wide teflon tape was centered along the inside length of the tack tape and was the material which actually made contact with the bondline. Both bonding surfaces of the butt joints were pre-wet with adhesive and placed in the jig in close proximity to what the final location would be.

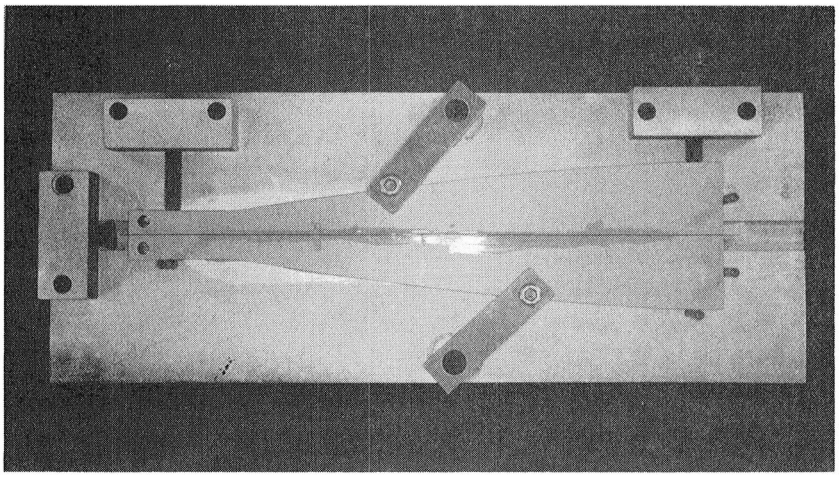

(a)

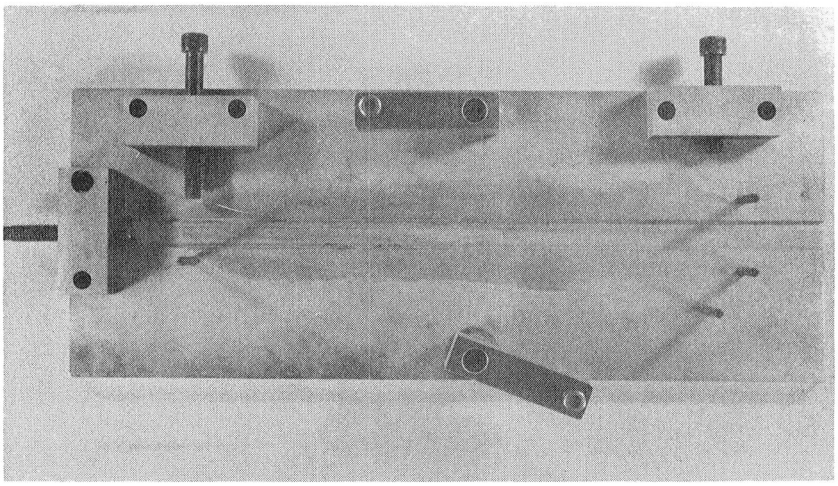

(b)

FIGURE 2-1. BONDING PROCEDURE FOR THE CONTOUR DOUBLE CANTILEVER BEAM. (a) SPECIMEN IN PLACE IN FIXTURE AND (b) FIXTURE ALONE.

Excess portions of the tack tape and teflon ribbon were immediately looped against the sides of the bondline as a dam, Figure 2-3. Removable shims were used at each side of the bond as the adherends were slid into proper position by the screw at the end of jig. When the correct bond width was obtained, the shims were removed and adhesive quickly filled the voids. Excess adhesive was removed with a spatula prior to room temperature precure. After partial cure was obtained (24 hours at room temperature and 1-2 days at 130°F) the joints were removed from the jig in preparation for post-cure. Examination of the bondline using neutron radiography[1] was done on selected specimens prior to postcure.

2.4 Non-Destructive Inspection

All bonded specimens were examined prior to post-cure and testing for obvious defects which might preclude their use. Loss of contact with the adhesive dam could produce an adhesive-starved joint and this and other bondline flaws could be eliminated at this point. The aluminum adherend test specimens were examined for flaw and void inclusions using neutron radiography. Most bondline defects, e.g., bubble inclusion and adverse surface wetting, were readily observable using this technique. The configuration of the cantilever beam specimen bondline required extraordinary mounting of the specimen within the neutron beam in order to project an image of sufficient width to ensure adequate detection of flaws. Projected bond widths varied from slightly more than 1.27 cm (0.5 inch) at top of the beam to just under 0.76 cm (0.3 inch) at the bottom of the beam , Figure 2-4. Correlation of extraneous artifacts (excess adhesive, dam material, teflon tape) on the surface of the specimen and film anomolies required careful interpretation in order to differentiate these areas from those of actual flaws. Representative radiographs are shown in Figure 2-4 depicting void inclusions as well as surface artifacts. Failed specimen surfaces showed good correlation between visual and N-ray detectable voids.

A neutron radiograph positive print of an aluminum butt joint is shown in Figure 2-5. This picture shows an acceptable joint on the right (also shows the transducer shoe mounts in place on this specimen) and an image of an unacceptable joint with void on the left. Correlations of N-ray data and visual examinations of failed surfaces were made after testing of the specimens.

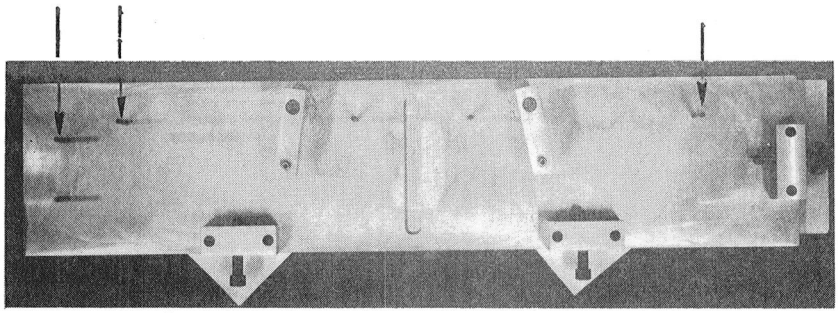

FIGURE 2-2. BUTT JOINT BONDING JIG.
NOTE GUIDE PINS.

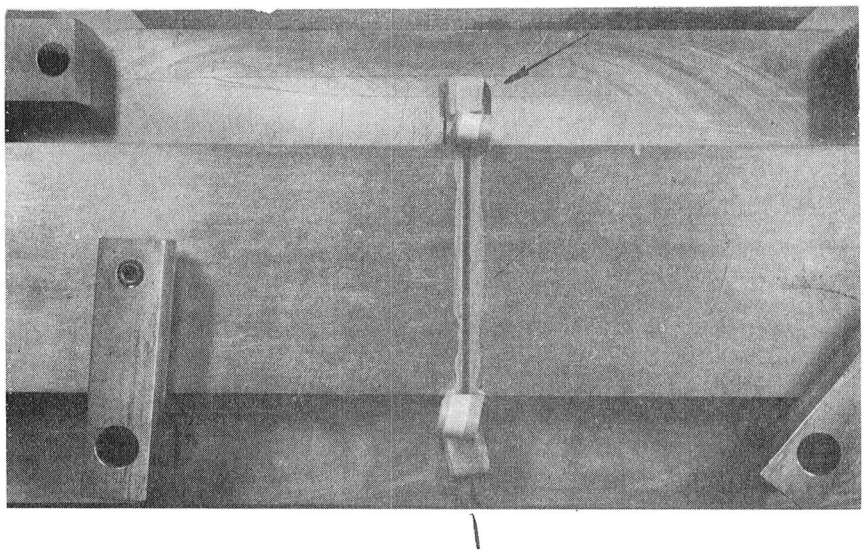

FIGURE 2-3. ALUMINUM BUTT JOINT SHOWING ADHESIVE DAM.
NOTE DAMMING MATERIAL.

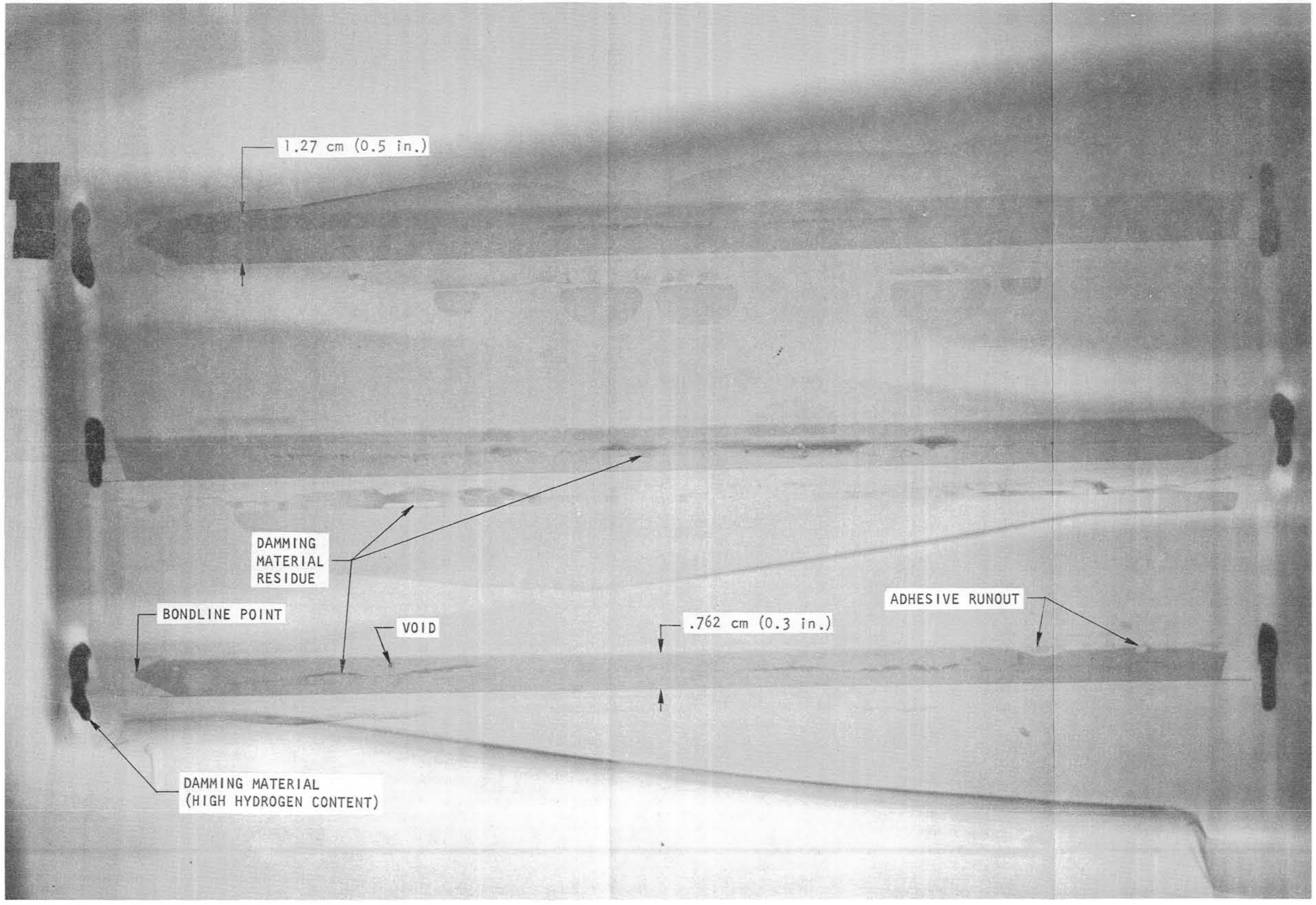

FIGURE 2-4. NEUTRON RADIOGRAPH OF THREE CONTOURED DOUBLE CANTILEVER BEAMS SHOWING SPECIMEN IMAGING AND INTERPRETATION.

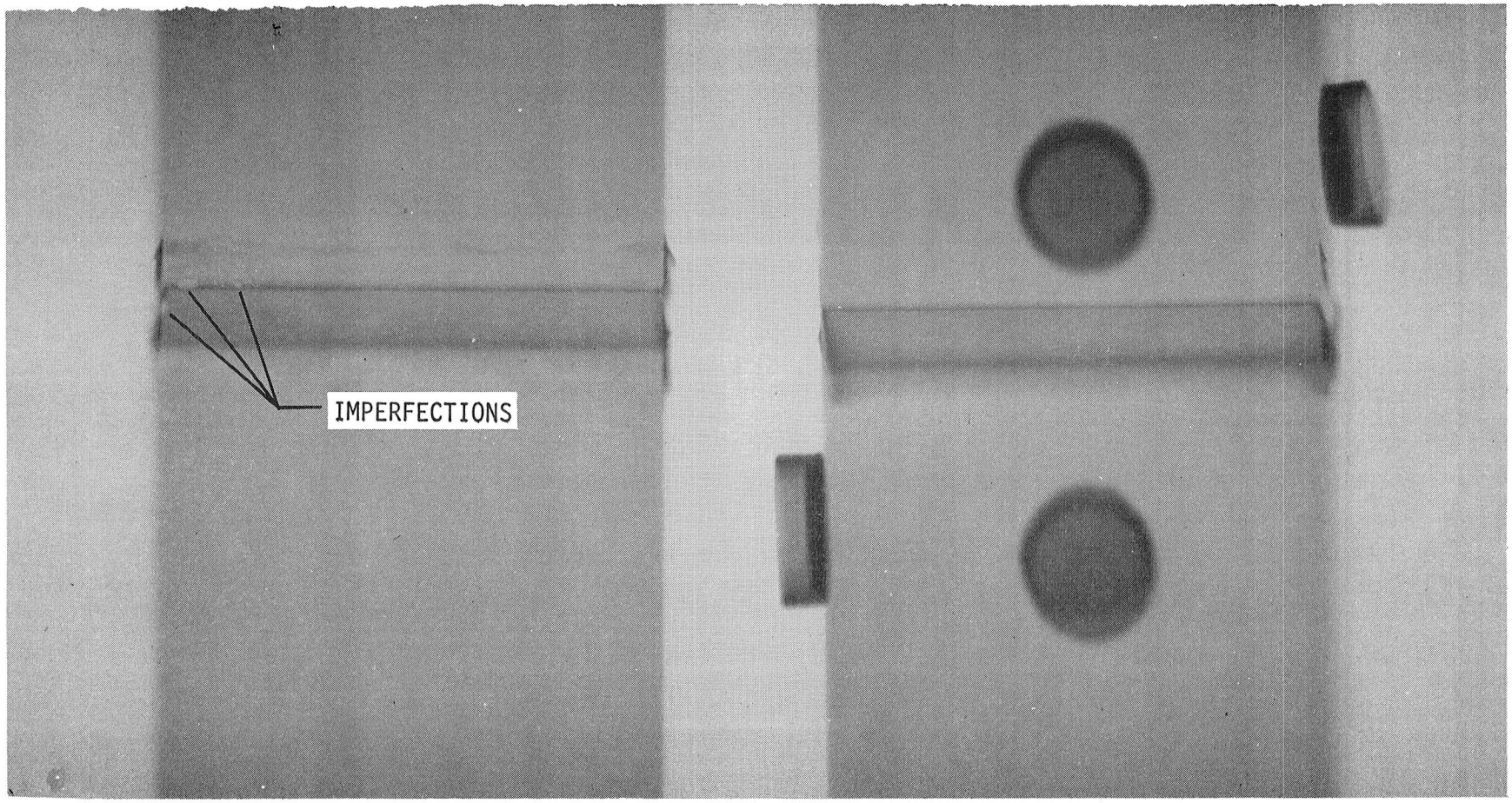

FIGURE 2-5. QUALITY ASSURANCE BONDLINE INSPECTION USING NEUTRON RADIOGRAPHY

3.0 ADHESIVE CHARACTERIZATION

3.1 Bulk Adhesive Tests

In addition to the adhesive selection criterion outlined in Section (2.1), the quality of the triaxial tensile stress state present in the adhesive bondline is also dependent on the mechanical properties of the adhesive, specifically, Poisson's ratio and Young's modulus. Therefore, a total of three 10.2 cm (4.0 inch) long dogbone bulk adhesive specimens were fabricated from each of the four candidate adhesives to facilitate tensile and fatigue testing. Two specimens of each adhesive were instrumented with longitudinal and transverse strain gages and pulled to failure in uniaxial tension to obtain E, ν and σ_{T_u}. Figure 3-1 shows the specimen mounted in the test machine. The average ultimate tensile stress for all tension tests was 34.37 MPa (5000 psi); on this basis the fatigue spectrum for the bulk adhesive specimens was determined to be 20% σ_{T_u} for 10,000 cycles (R = + 0.1 η = 3 Hz) followed by 5000 cycles each at 30%, 40%, 60% and 70% σ_{T_u}. The results of these tests are reported in Table 3-1. On the basis of these tests and the data presented in Tables 2-1, 2-2 the HYSOL 9313 adhesive system was selected. It is important to note that one of the prime considerations in adhesive selection was transparency for visual observation of crack initiation and growth. Inherent problems found to exist in bonding acrylics with epoxy adhesives precluded visual monitoring of flaw propagation and subsequent completion of the lucite specimens. However, this occurred at a point in the program where alternate adhesive selection was no longer practical.

3.2 Double Cantilever Beam Specimen Tests

The aluminum contoured double cantilever beam specimens were pin loaded on a 20,000 pound capacity CGS Testing Machine in the Vought Advanced Technology Center Laboratory, Figure 3-2. Since the bondline extended well into the untapered portion of the specimen, the crack had to be initiated and propagated to the threshold (beginning of contour), Figure 3-3. Crack initiation was accomplished by a monotonically increasing tensile load at a rate of 8.9 N/sec (120 lb/min). The load required varied between 2.00-2.89 kN (450-650 lbs) characteristically, depending on the length of the bondline and the condition of the point at the bondline tip. After initiation, the crack was propagated at a stress ratio, R, of + 0.1 and a load equal to 50% of the initiation load.

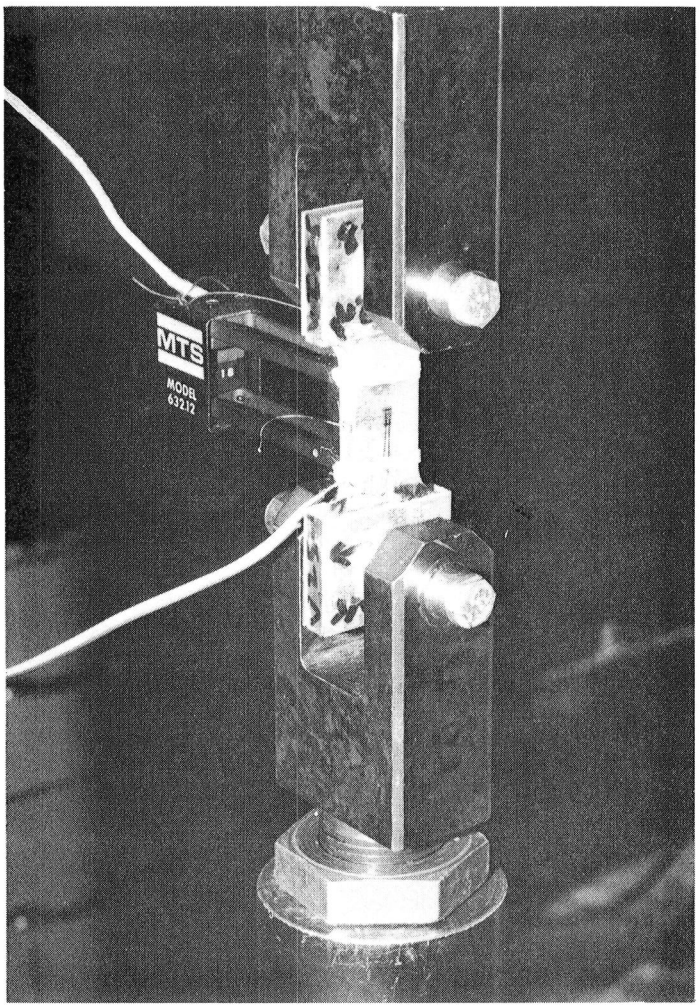

FIGURE 3-1. BULK ADHESIVE SPECIMEN MOUNTED IN TEST MACHINE.

TABLE 3-1. BULK ADHESIVE TEST RESULTS

ADHESIVE SYSTEM	STATIC			FATIGUE	
	AVERAGE MODULUS GPa(KSI)	POISSON'S RATIO	AVERAGE ULTIMATE TENSILE STRENGTH MPa (KSI)	MAX STRESS MPa (PSI) R = +0.1	# CYCLES
Epon 828-DTA	1.5513 (225.00)	0.30	28.751 (4.17)	6.895 (1000)	10,000
				10.342 (1500)	5,000
				13.789 (2000)	430*
Epon 828-V140	0.9873 (143.20)	0.20	31.785 (4.61)	6.895 (1000)	10,000
				10.342 (1500)	5,000
				13.789 (2000)	5,000
				20.684 (3000)	492*
Epon 828-V25	1.8747 (291.90)	0.26	34.129 (4.95)	6.895 (1000)	10,000
				10.342 (1500)	5,000
				13.789 (2000)	5,000
				20.684 (3000)	5,000
				24.132 (3500)	4,844*
Hysol 9313	1.1162 (161.90)	0.80**	35.370 (5.13)	6.895 (1000)	10,000
				10.342 (1500)	5,000
				13.789 (2000)	5,000
				20.684 (3000)	5,000
				24.132 (3500)	3,010*

*Failure Occurred
**Questionable Data

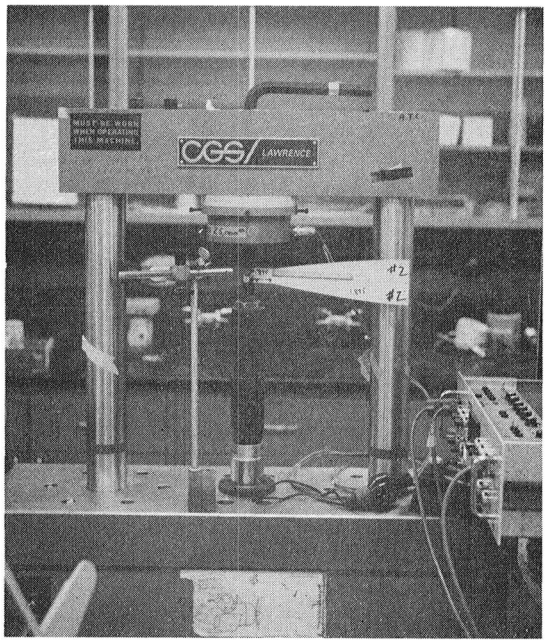

FIGURE 3-2. CANTILEVER BEAM SPECIMEN MOUNTED IN TEST MACHINE.

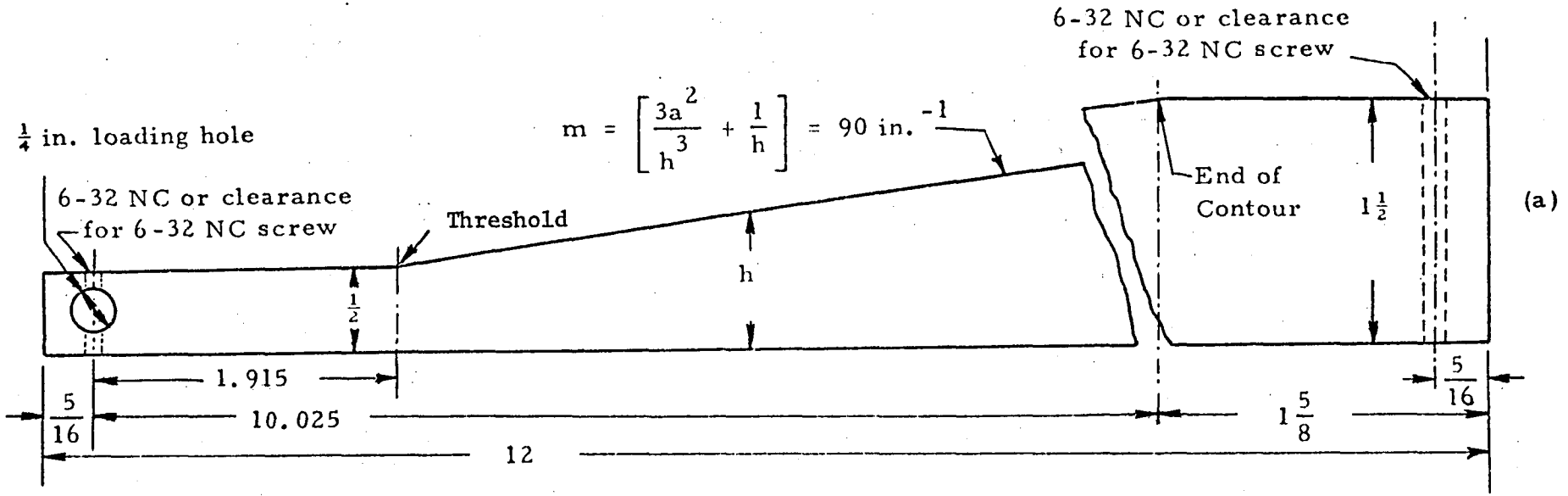

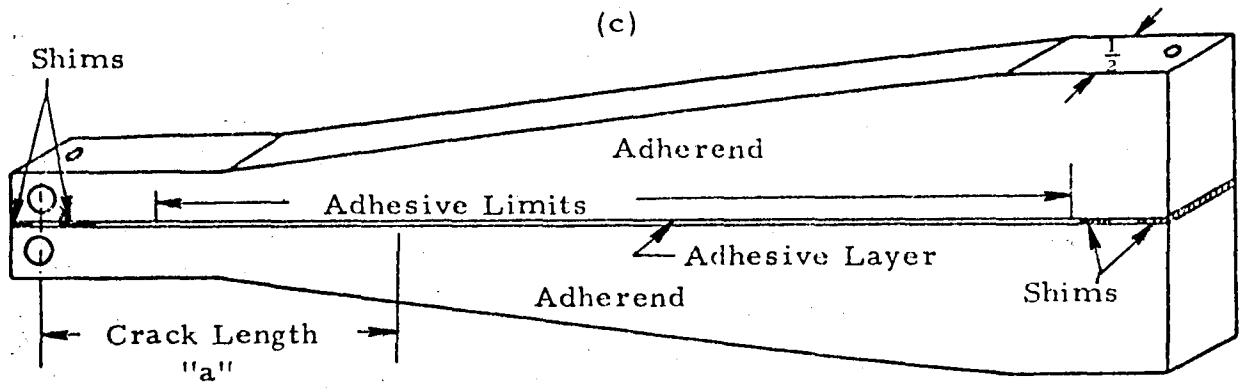

Crack Length, a vs. Height, h inches	
a	h
1.915	0.500
2.000	0.515
3.000	0.674
3.750	0.781
5.000	0.945
6.000	1.066
7.000	1.181
8.000	1.291
9.000	1.396
10.000	1.498
10.025	1.500

(b)

Figure 3-3. Contoured Double Cantilever Beam (CDCB) Test Specimen Drawings and Table. (a) Single Adherend with Dimensions Prior to Bonding. (b) Crack Length, a vs, Height, h, for $m = 90$ in^{-1} Contour. (c) Bonded Adhesive Test Specimen.[21]

Upon reaching the threshold, the crack was propagated at the load levels and stress intensity factors shown in Table 3-2; the stress ratio was preserved. For contour double cantilever beam specimens, $K = (2P/b)\sqrt{m}$, (Ref. 2), where P is the load, b is the specimen width and m is the contour coefficient.[3]

Visual data in the form of crack length, a, versus number of cycles, N, was recorded as the crack propagated to a length of approximately 10.2 - 12.7 cm (4 to 5 inches). At this point a tensile load was again applied to separate the specimen halves for purposes of examining the fracture surface. Figure 3-4 (a) and (b) compare the fracture surface of the fatigue and tensile portions, respectively, using 100X scanning electron microscopy with backscatter electrons. These observations can be made from this figure: The fatigue portion of the beam resulted in proportionally smaller stress-induced voids of higher population density than the tensile portion; the surface striations radiate from void centers on the fatigue portion but are oriented randomly after tensile loading. From these examinations the average void size was determined to be .0043 cm (.0017 in) and .0057 cm (.0022 in) under fatigue and tensile loading, respectively.

Test data were reduced in the form of crack length versus number of cycles curves as represented in Figure 3-5. The slope at the beginning of the contour in this figure is seen to differ from the slope of the remainder of the test. This is caused by the transitioning of the stress state into the constant stress intensity environment of the contoured portion of the beam and can be thought of as an "edge effect" whose length is less than the specimen thickness for all tests. This phenomenon, however, had no influence on the test results.

From each of the four load levels (Table 3-2), the slope (da/dN) and the difference in stress intensity factors (ΔK) can be calculated in order to generate a da/dN versus ΔK plot as in Figure 3-6. This provided the necessary input to the fatigue life prediction theory in the form of the parameters c and q which are the ordinate intercept and slope of the plot, respectively. The parameters were then input to the power-law crack growth relation which is the basis of the fatigue failure theory.

TABLE 3-2

CANTILEVER BEAM LOAD LEVELS
AND STRESS INTENSITY FACTORS

SPECIMEN NO.	MAX LOAD, P_{max} N (lbs)	MAX STRESS INTENSITY, K_{max} MPa $\sqrt{m}$ (psi $\sqrt{in}$)	$K_{max} - K_{min}$ ΔK MPa $\sqrt{m}$ (psi $\sqrt{in}$)
1, 2	889.6 (200)	8.34 (7589.5)	7.51 (6830.5)
3, 4	800.6 (180)	7.51 (6830.5)	6.76 (6147.5)
5, 6	978.6 (220)	9.17 (8348.4)	8.26 (7513.6)
7, 8	667.2 (150)	6.25 (5692.1)	5.63 (5122.9)

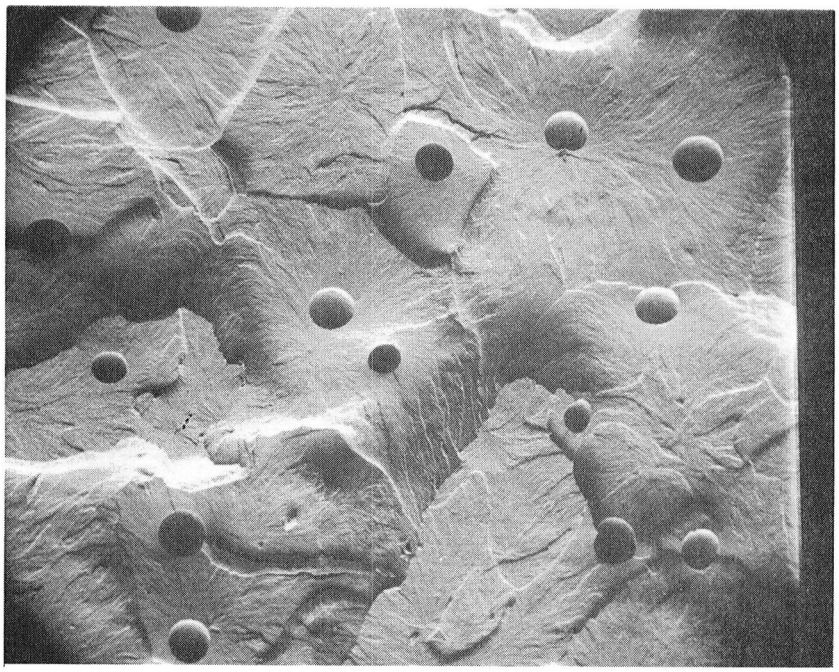

(a)

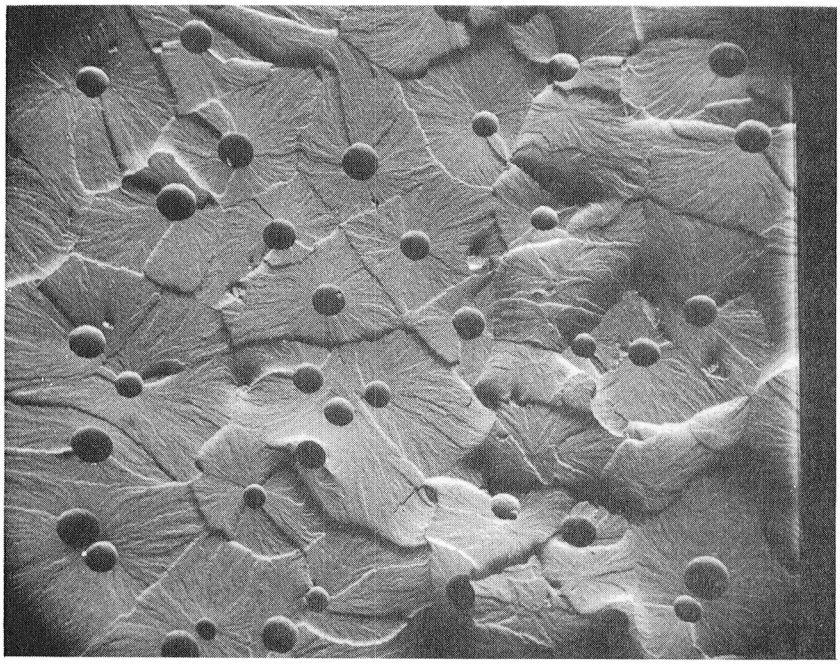

(b)

FIGURE 3-4. FAILURE SURFACES OF THE CANTILEVER BEAM SPECIMENS UNDER (a) TENSILE AND (b) FATIGUE LOADING USING 100X BACK-SCATTER SCANNING ELECTRON MICROSCOPY

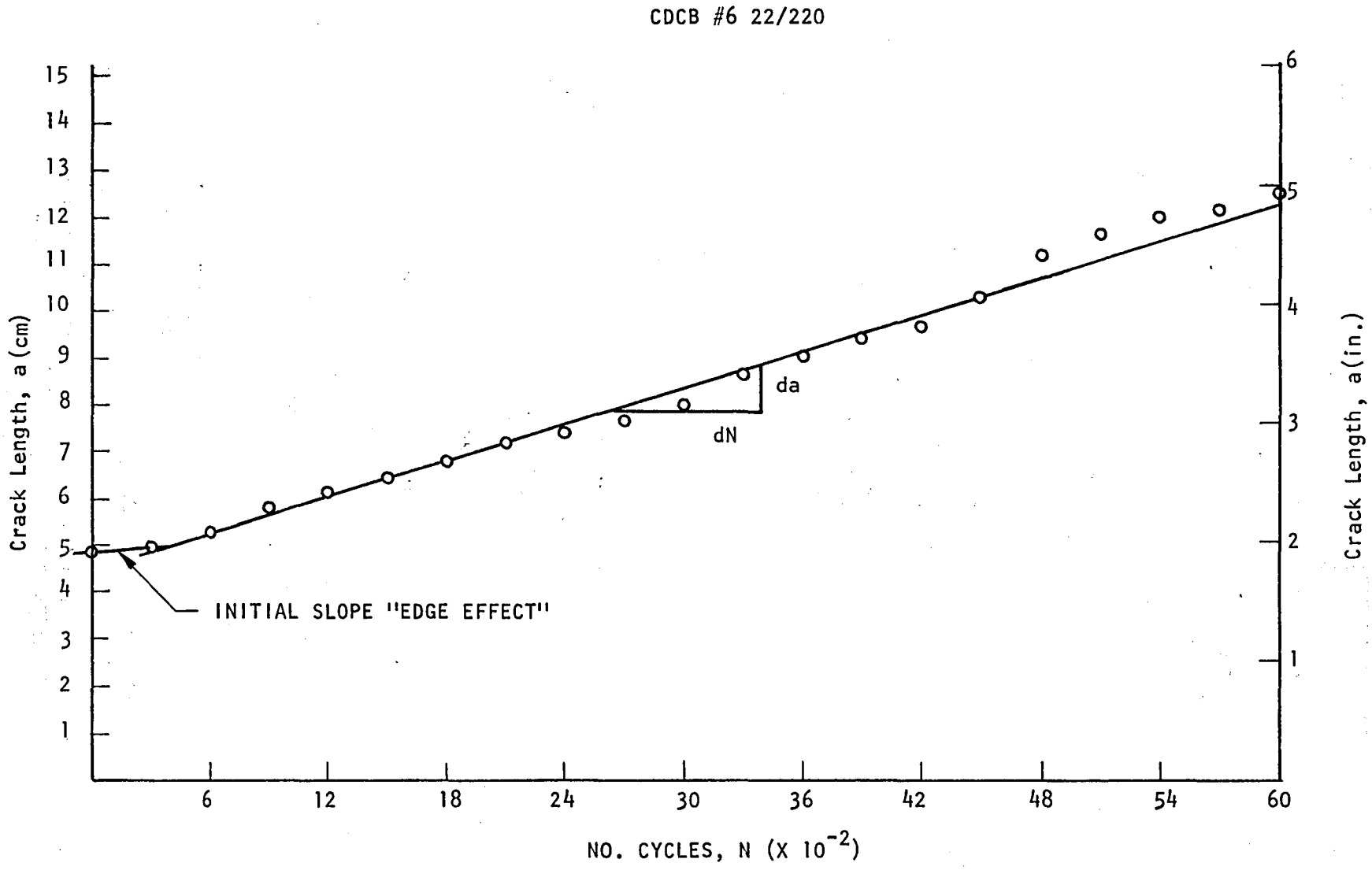

FIGURE 3-5. CRACK LENGTH VERSUS NUMBER OF CYCLES FOR A CONTOUR DOUBLE CANTILEVER BEAM SPECIMEN CYCLED BETWEEN 3.1 AND 31 NEWTONS (22 AND 220 POUNDS).

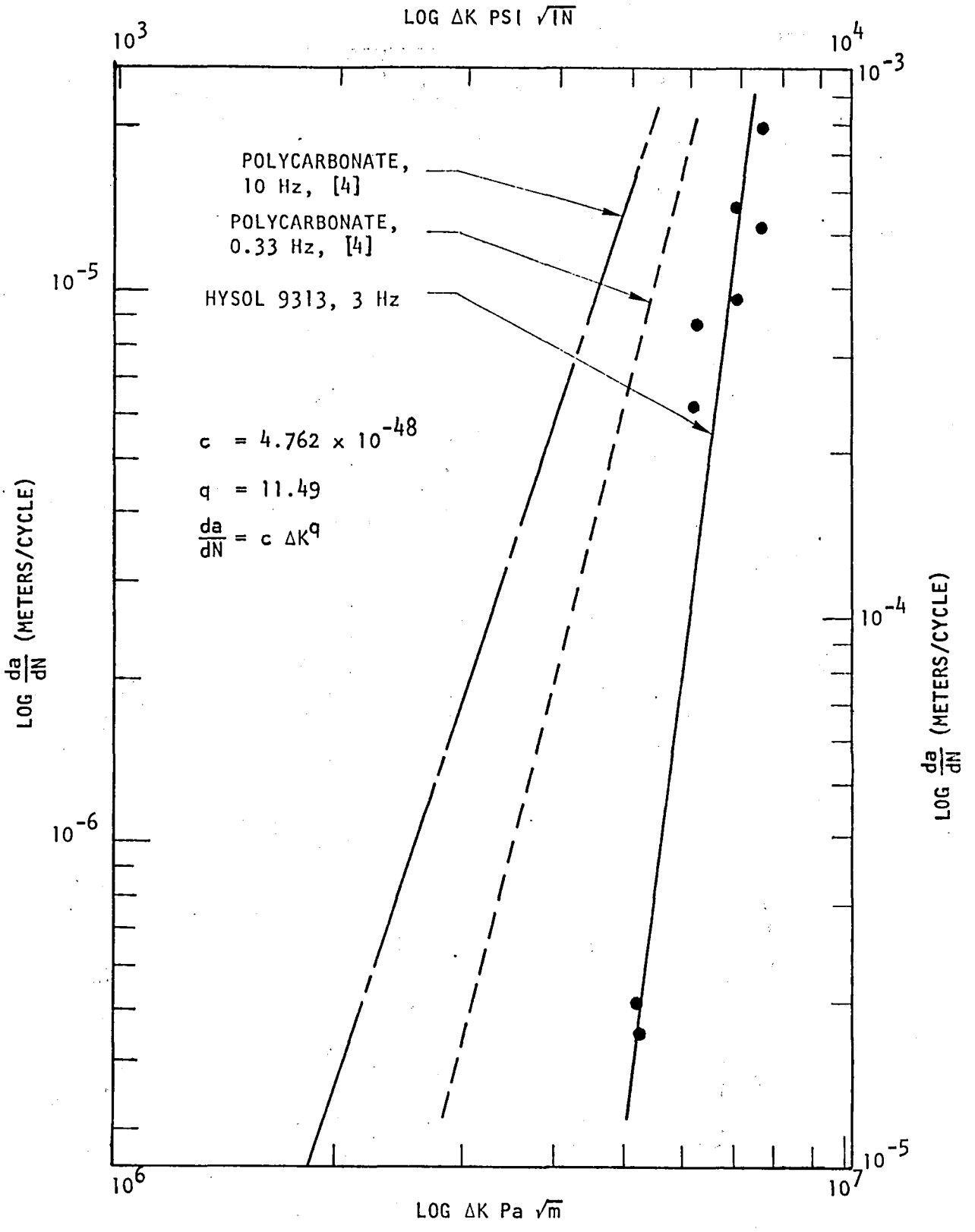

FIGURE 3-6. da/dN VERSUS ΔK FOR HYSOL 9313 AS COMPARED TO THAT OF POLYCARBONATE, ANOTHER THERMOSET POLYMER

4.0 MECHANICAL TESTING

This program involved both the definition of an analytical methodology and the generation of the experimental data base for verifying the model. In order to demonstrate the applicability of the fatigue failure analysis, experimental measurements were made by mechanically testing aluminum butt/scarf joint and graphite/epoxy butt joint specimens. The measurements needed from these tests included local failure time, t'_f, global failure time, t_f, as well as number of cycles to failure, compliance change, and acoustic emission response. The details of the experimental program and the analysis of the fatigue data are outlined in the section below.

4.1 Test Specimen Configuration

The introduction of a uniform triaxial tensile state over a large portion of the bondline was the primary driver of specimen geometry. Proper relationships had to be maintained between specimen length and bondline dimensions. At the same time, the design had to be compatible with acoustic emission instrumentation. Specimen dimensions were determined form a closed-form analytical model which sizes the specimen to maximize the extent of the uniform stress (strain) region in the adhesive.[5] Figure 4-1 illustrates the effect of adhesive/adherend properties on the stress state presented as the normalized average normal stress versus distance from the bondline center (in terms of percent of aspect ratio). Figure 4-2 is a similar plot for the selected joint configuration (Figure 4-3) of 60.96 cm (24 inches) in adherend length and bondline dimensions of 0.03 x 1.90 x 7.62 cm (0.010 x 0.75 x 3.0 inches) for the thickness, width and length, respectively. As can be seen from this figure, the inplane stress components, σ_s, σ_z, are equal in magnitude over 90% of the bond length and approximately 20% as large as the normal stress, σ_n.

The experimental portion of the program consisted of constant amplitude fatigue testing of fifteen (15) aluminum butt joint, fifteen (15) graphite/epoxy butt joint and five (5) aluminum scarf joint specimens. In addition, fifteen (15) tests were performed to verify test procedures and establish load ranges. The stress ratio, R, and frequency, η, of the tests were +0.1 and 10 Hz, respectively.

The compliance response of the butt and scarf joints was measured with an MTS extensometer of 2.54 cm (1.0 inch) gage length throughout each test and recorded with a Hewlett Packard oscillographic recorder. The compliance of the bondline

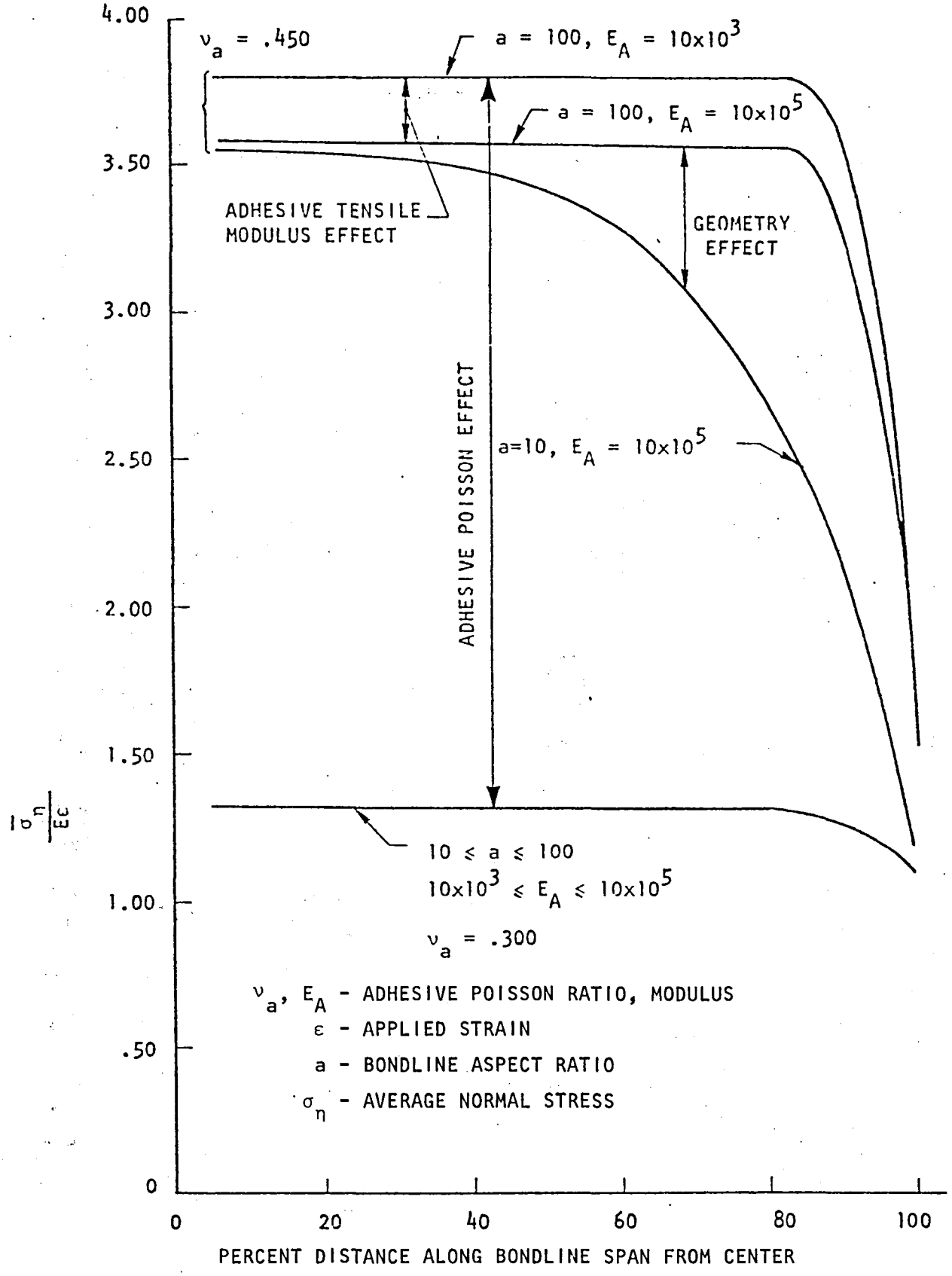

FIGURE 4-1. PRIMARY NORMAL STRESS DISTRIBUTION IN SCARF(BUTT) JOINTS AS DETERMINED BY ANALYTICAL MODEL. (REFERENCE 5)

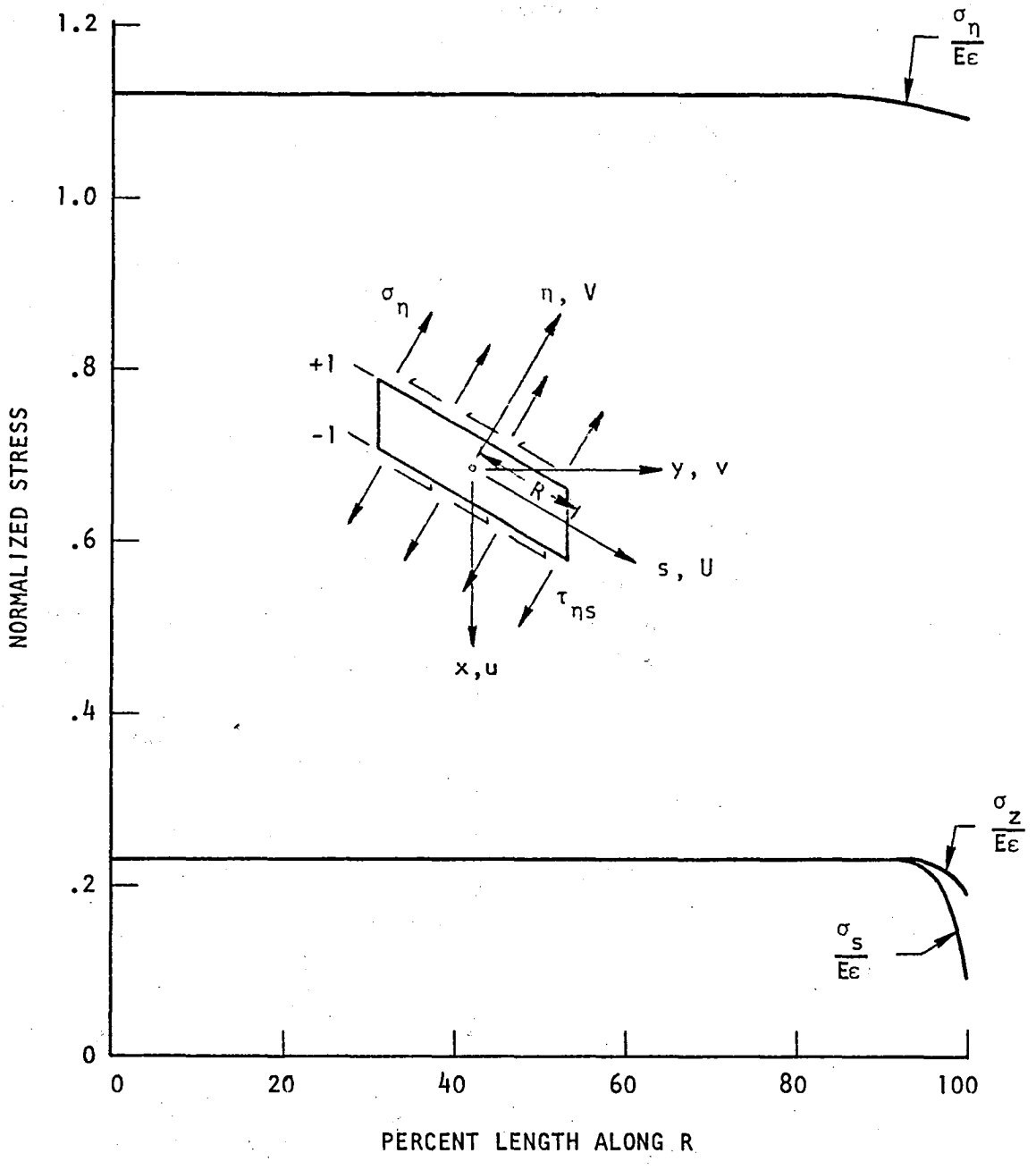

FIGURE 4-2. NORMALIZED STRESS DISTRIBUTION FOR SPECIMEN CONFIGURATION AND THICKNESS CROSS-SECTION OF BONDLINE SHOWING SCARF JOINT COORDINATE SYSTEMS (Z AXIS OUT-OF-PLANE).

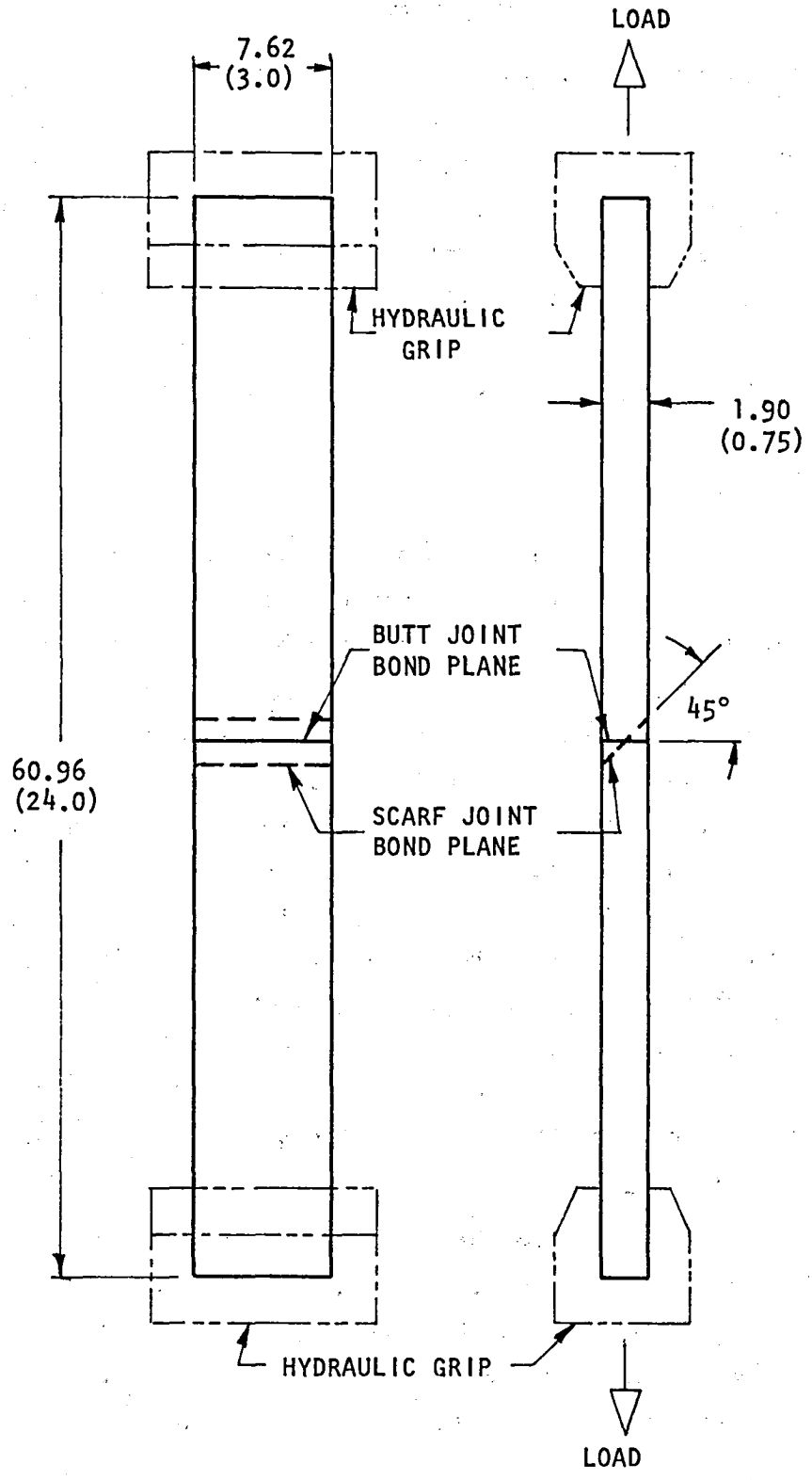

FIGURE 4-3. BUTT AND SCARF JOINT SPECIMEN AND LOAD CONFIGURATIONS. 0.03 (0.01 INCH) ADHESIVE THICKNESS.

remained constant up until 2-3 seconds before catastrophic failure, at which point slight increases were noted. These increases were not relatable to the acoustic response because of the relatively short time over which the compliance change could be measured.

The determination of the proper stress level at which to cycle the butt and scarf joints proved to be a particularly challenging task due to the steep slope of the Rate-K curve, Figure 3-6. Clearly the crack growth rate is highly sensitive to stress level. In essence, there exists a narrow band of load levels for stable crack growth below which crack propagation occurs very slowly or not at all, and above which catastrophic failure occurs instantaneously with crack initiation. The triaxial nature of the bondline stress state made failure stress correlations with previously run uniaxially-stressed bulk adhesive specimens difficult due to the lack of information as to the inherent flaw size in the adhesive bondline. The fact that the bulk adhesive tension specimen failed uniaxially at approximately 34.47 MPa (5.0 ksi) could not be used to determine that a triaxially stressed butt joint bondline of the same adhesive would fail at an acceptable number of cycles and a stress level of 28.96 MPa (4.2 ksi) which testing proved. This stress level was determined by beginning the aluminum butt joint fatigue tests at a stress equal to one-half the uniaxial tension failure stress (17.24 MPa (2.5 ksi)) and systematically raising the load 10 percent every 1 ~ 2 x 10^4 cycles until failure. Once the stress level was increased, however, the specimen could not be considered part of the test package because the test was no longer constant amplitude.

4.2 Failure Surface Observations

Post-test failure analysis by visual inspection of the surfaces provided many clues as to the sequence of failure of the adhesive bondlines in their butt and scarf joint configurations. Much of what was observed was correlated with the acoustic emission response presented in Section 5 to better understand the mode of failure. Epoxy resin systems, and particularly HYSOL 9313, respond quite differently to fatigue loading than the stable crack growth characteristic of metals which results in a clearly definable crack initiation site and can be tracked by the striated surface left by a growing crack.

The aluminum butt joints showed the most consistent failure surface character. The center portion of the fracture surface was stress-whitened (crazed) and gave

a peppered appearance due to the growth of stress-induced voids with applied load. The whiteness indicated the presence of microvoids which develop during the orientation of groups of polymeric chains within the epoxy parallel to the applied load. These chains, or fibrils, are regions of high plasticity and the increase in localized surface area which accompanies fibril formation increases the refractivity of the surface resulting in a whitened appearance. The disappearance of the whitened area upon heating was further evidence of high localized plasticity (crazing). Figure 4-4 depicts a typical fracture surface of an aluminum butt joint. Surrounding the crazed region and extending to all planar boundaries of the bondline is an area of rapid crack growth resulting in translucent material which contains a smaller population of induced voids and which is macroscopically similar to the fracture surface of the unstable crack growth portion of the cantilever beam specimens.

In contrast to the aluminum butt joints, failure initiated in the graphite/epoxy butts either along the bondline short dimension or at a corner in every case. The differences in failure mode between the graphite/epoxy and aluminum butt joints indicated the profound effect of adherend material. The more localized failure of the graphite/epoxy adherend joints suggests the presence of higher stress concentration or energy release rate at the bondline edges of these specimens. It is conceivable that the lower principal in-plane shear modulus and shear strength of the graphite/epoxy influenced the stress intensity of the initial edge flaws by allowing greater crack-opening displacement, but this phenomenon can only be understood with a detailed stress analysis of the different joints which was not within the scope of this program. A typical graphite/epoxy butt joint failure surface is shown in Figure 4-5.

The failure surface of the aluminum scarf joint differed significantly from that of the butt joints. Crazing appeared in the center of the bondline as in the aluminum butts, however, instead of having a "plateau-type" topography, the surface was a series of overlapping membranes. Brussat[6] observed the same phenomenon on the failure surface of Mode III modified zero K-gradient specimens. The surface appeared to be composed of a series of small cracks propagating out of the plane of the 45° scarf and blunting at the aluminum adherend interface. The width of the cracks coincided with the long dimension of the bondline. Looking down the length of the scarf bond-plane, the membranes lay upon each other in a "domino" fashion oriented in a direction which appeared to be

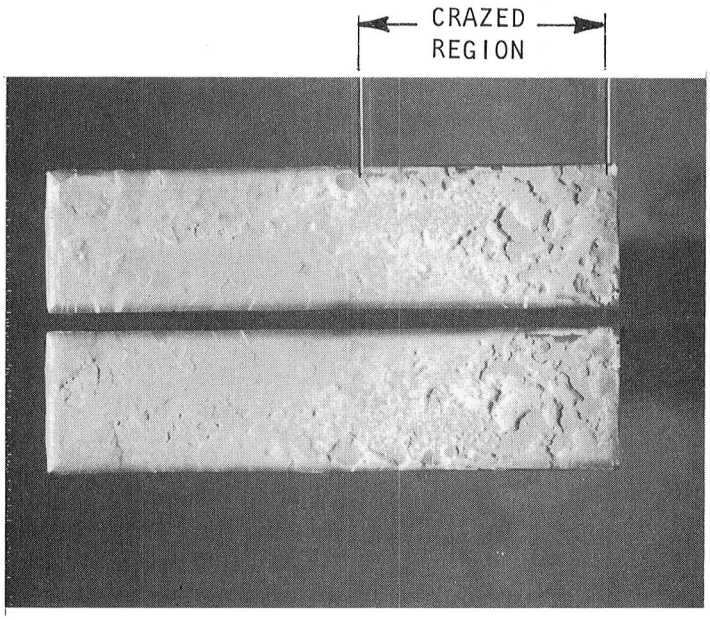

FIGURE 4-4 PHOTOGRAPH OF A TYPICAL FAILURE SURFACE OF AN ALUMINUM BUTT JOINT (SPECIMEN AB-21)

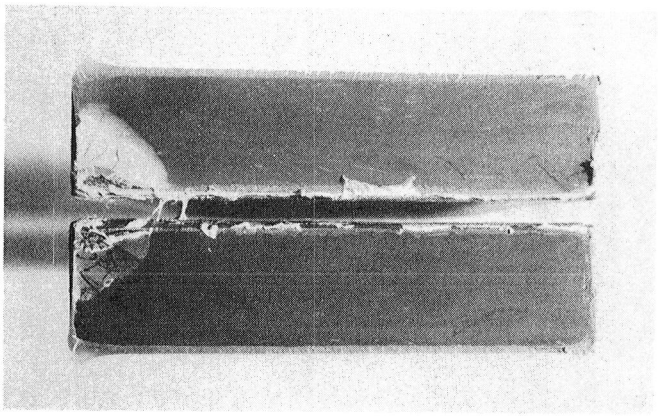

FIGURE 4-5 PHOTOGRAPH OF A TYPICAL FAILURE SURFACE OF A GRAPHITE/EPOXY BUTT JOINT (SPECIMEN GB-9).

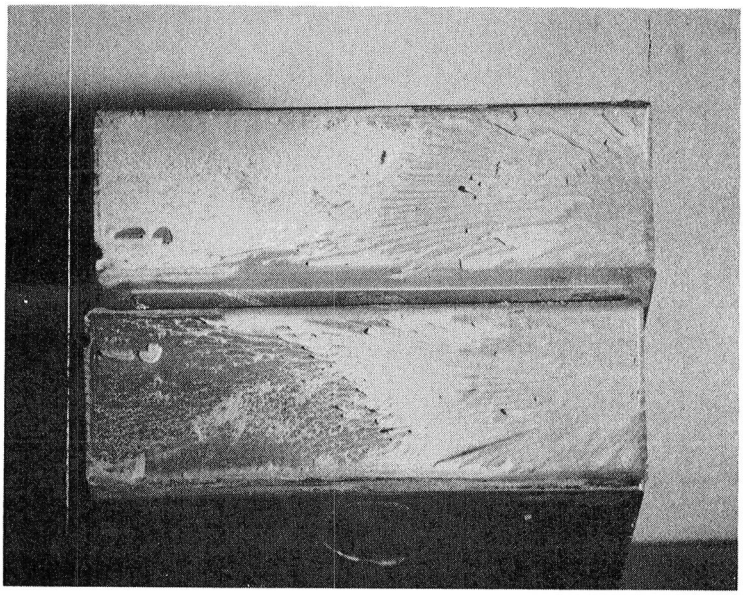

FIGURE 4-6 PHOTOGRAPH OF A TYPICAL FAILURE SURFACE OF AN ALUMINUM SCARF JOINT. VIEW IS PERPENDICULAR TO SURFACE. (SPECIMEN AS-5)

perpendicular to the maximum principal stress. Figure 4-6 shows the failure surface which was typical of an aluminum scarf joint.

4.3 Analysis of Fatigue Data

In order to determine the applicability of the proposed fatigue failure theory, the results of the mechanical tests require reduction and interpretation. The fatigue data are analyzed below in accordance with the theory presented in Appendix A. A direct result of the testing is that if the dominant crack in each specimen does not start as a macrocrack, the number of cycles required to produce a macrocrack from a microcrack or other type of microflaw is at least negligible, i.e. $t'_f \tilde{=} 0$ and $t_f \propto N_f$, compared to the fatigue life of the specimen. This fact is supported by the data as presented in this section.

Tables 4-1 and 4-2 give the butt and scarf joint fatigue lifetimes in terms of the natural log of the number of cycles N and the "reduced-life" parameter $\tilde{N}$, Equation (A-18). The CDCB tests provided the value of q = 11.49, which was used to calculate $\tilde{N}$ for each value of stress amplitude $\Delta\sigma_j$. Inasmuch as all specimens had the same bonded area, the load amplitudes ΔL_j could be used in Equation (A-18). Thus,

$$\tilde{N}_j = \left(\frac{\Delta L_j}{\Delta L_1}\right)^{11.49} N \qquad (4\text{-}1)$$

where ΔL_1 = 8100 (pounds) for these calculations. The cumulative distribution of failures was plotted using Weibull probability paper as shown in Figure 4-7. The data in Table 4-1 for the aluminum butt joints show good dispersion of specimen load levels when ordered by increasing $\ln \tilde{N}$. This indicates that the value of q is realistic; the linear character of Figure 4-7 further supports the premise that the failure theory accurately models the fatigue failure of these specimens. The graphite/epoxy data reported in Table 4-2, however, display a very segregated nature in specimen load levels when listed in order of increasing lifetime, $\ln \tilde{N}$. (low load levels result in short lifetimes, etc.). This phenomenon could be caused by an improper q value, but since the q is shown to be accurate in the aluminum butt data, the result tends to suggest a different fracture mechanism. Evidence of a different mode of failure occurring in the graphite/epoxy specimens is also supported by the fracture surface examination (Section 4.2) and the low level acoustic emission response (Section 5.3). Since the aluminum butt joint data could be fit quite well by a straight line, the failure probability function,

TABLE 4-1 FAILURE SEQUENCES FOR ALUMINUM JOINTS

ORDER	ACTUAL SEQUENCE SPECIMEN	MAX LOAD kN (kip)	ln N	REDUCED LIFE SEQUENCE SPECIMEN	MAX LOAD kN (kip)	ln $\tilde{N}$
ALUMINUM BUTT JOINTS						
1	AB 20	51.15 (11.5)	10.55	AB 12	40.03 (9.0)	11.54
2	21	51.15 (11.5)	11.13	11	40.03 (9.0)	12.07
3	12	40.03 (9.0)	11.54	16	40.03 (9.0)	12.41
4	18	51.15 (11.5)	11.90	22	42.70 (9.6)	12.71
5	22	42.70 (9.6)	11.97	13	40.03 (9.0)	12.97
6	19	51.15 (11.5)	11.97	17	41.37 (9.3)	13.15
7	11	40.03 (0.0)	12.07	6	42.26 (9.5)	13.24
8	16	40.03 (9.0)	12.41	20	51.15 (11.5)	13.37
9	6	42.26 (9.5)	12.62	10	42.70 (9.6)	13.39
10	10	42.70 (9.6)	12.65	15	37.81 (8.5)	13.45
11	17	41.37 (9.3)	12.77	5	40.03 (9.0)	13.49
12	13	40.03 (9.0)	12.97	8	42.70 (9.6)	13.94
13	8	42.70 (9.6)	13.20	21	51.15 (11.5)	13.95
14	7	42.70 (9.6)	13.22	7	42.70 (9.6)	13.97
15	9	42.70 (9.6)	13.23	9	42.70 (9.6)	13.97
16	5	40.03 (9.0)	13.49	18	51.15 (11.5)	14.71
17	15	37.81 (8.5)	14.10	19	51.15 (11.5)	14.97
ALUMINUM SCARF JOINTS						
1	AS 6	46.70 (10.5)	11.83	AS 2	35.58 (8.0)	10.30
2	5	46.70 (10.5)	12.03	4	44.48 (10.0)	11.57
3	4	44.48 (10.0)	12.13	3	40.04 (9.0)	11.65
4	2	35.58 (8.0)	13.41	6	46.70 (10.5)	11.83
5	3	40.03 (9.0)	13.42	5	46.70 (10.5)	12.03

TABLE 4-2 FAILURE SEQUENCE FOR GRAPHITE/EPOXY BUTT JOINTS

ACTUAL SEQUENCE					REDUCED LIFE SEQUENCE				
ORDER	SPECIMEN	MAX LOAD kN	(kip)	ln N	SPECIMEN	MAX LOAD kN	(kip)	ln $\tilde{N}$
1	GB 1	42.70	(9.6)	7.64	GB 7	22.24	(5.0)	2.97
2	7	22.24	(5.0)	9.07	4	22.24	(5.0)	3.74
3	4	22.24	(5.0)	9.84	5	22.24	(5.0)	4.54
4	15	37.81	(8.5)	10.59	6	22.24	(5.0)	5.10
5	5	22.24	(5.0)	10.64	3	22.24	(5.0)	6.04
6	13	37.81	(8.5)	10.89	8	22.24	(5.0)	7.92
7	6	22.24	(5.0)	11.19	10	26.29	(6.0)	8.50
8	16	37.81	(8.5)	12.01	9	26.69	(6.0)	8.55
9	3	22.24	(5.0)	12.14	1	42.70	(9.6)	9.04
10	10	26.69	(6.0)	12.51	15	37.81	(8.5)	10.59
11	9	26.69	(6.0)	12.55	13	37.81	(8.5)	10.89
12	17	37.81	(8.5)	12.55	16	37.81	(8.5)	12.01
13	14	37.81	(8.5)	13.04	17	37.81	(8.5)	12.55
14	8	22.24	(5.0)	14.01	14	37.81	(8.5)	13.04
15	11	Failed in Test Machine Power Surge						

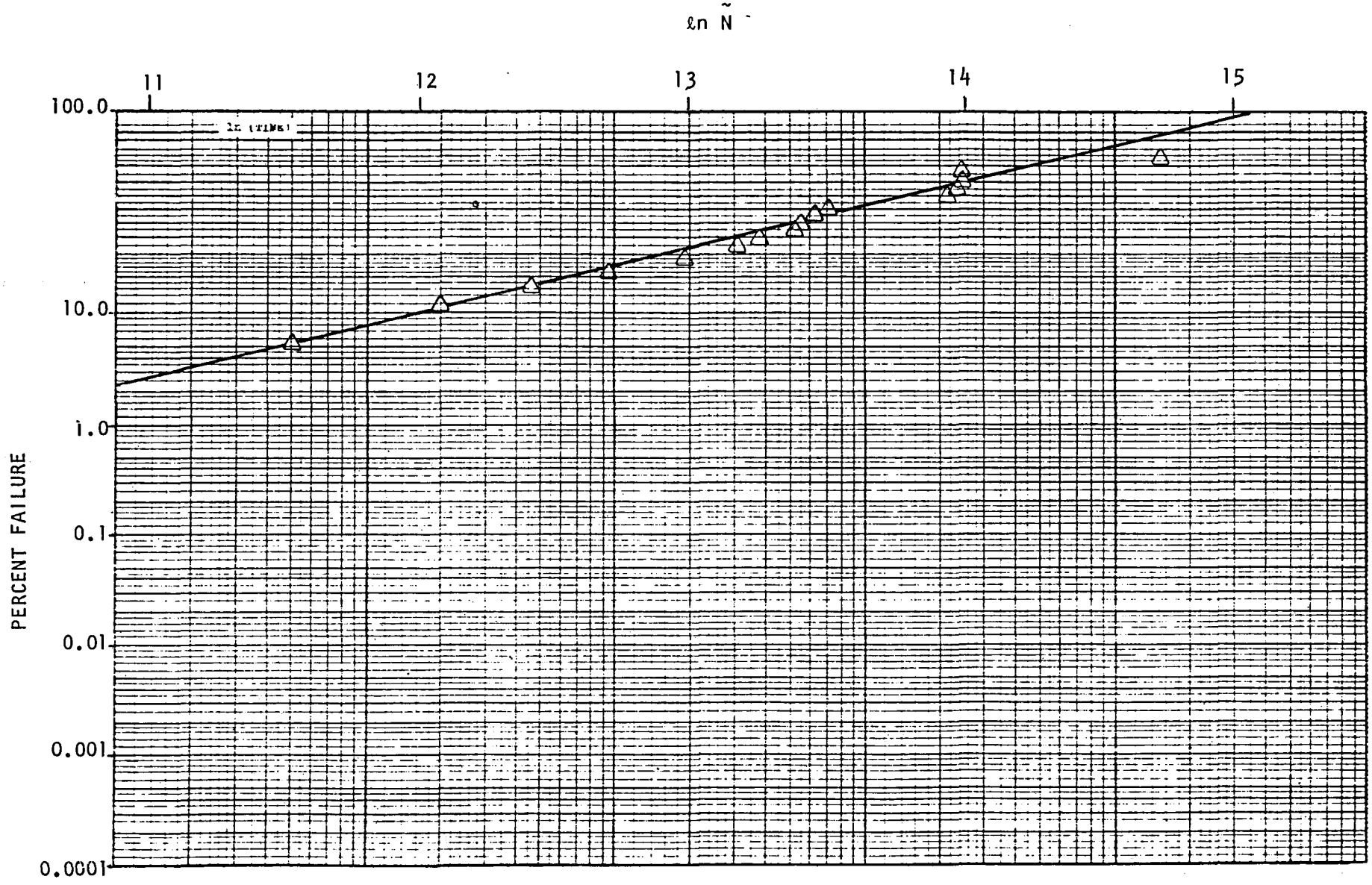

FIGURE 4-7 CUMULATIVE DISTRIBUTION FUNCTION FOR ALUMINUM BUTT JOINTS

Equation (A-15), becomes

$$P_f\ (0 \leq N \leq N_T) = 1 - \exp\ [-(\tilde{N}/\tilde{N}_o)^b] \qquad (4\text{-}2)$$

where, from the graph,

$$b = 1.39,\ \tilde{N}_o = 830{,}680. \qquad (4\text{-}3)$$

This value of the "shape parameter", b, is comparable to that reported for fatigue of fiber-reinforced epoxy.[7]

In principle, one can use these results to predict failure under variable amplitude loading if C = K = 1 in Equation (A-16). For this case, $\Delta L = \Delta L(N)$ and

$$\tilde{N} = \int_o^N \left(\frac{\Delta L}{\Delta L_1}\right)^q dN \qquad (4\text{-}4)$$

would be substituted into Equation (4-2) along with the parameters in Equation (4-3). Further experimental studies involving constant and variable amplitude loading are needed to determine whether or not C = K = 1 and, more specifically, to check the validity of Equation (4-4).

At this point, it was valuable to use these results to verify the assumption that the dominant crack is large relative to bondline thickness during most of the fatigue life. For this purpose, we used Equation (A-7), in which c and q are the parameters found for crack growth in the CDCB tests; specifically, with c, k, and q assumed constant,

$$N_f\ Ck^q(\Delta\sigma)^q = (pa_o^b)^{-1}. \qquad (4\text{-}5)$$

The adhesive bondline was approximately 7.6 cm long x 1.9 cm wide x 0.025 cm thick (3.0 x 0.75 x 0.01 inches). Thus, with $\Delta\sigma = \Delta\sigma_1$,

$$\Delta\sigma_1 = \frac{\Delta L_1}{3 \times .75} = \frac{8100}{3 \times .75} = 3600 \text{ psi}$$

For the sake of illustration, we used, for N_f the mean fatigue lifetime, $P_f = 0.5$; Equation (4-2) then yields $\tilde{N}_f \approx 638{,}000$ cycles; note that $\tilde{N} = N$ for this case since $\Delta\sigma = \Delta\sigma_1$. Also, from Figure 3-6 for the CDCB specimens,

$$c = 0.5 \times 10^{-47}, \quad q = 11.49$$

and

$$p = \frac{q}{2} - 1 = 4.75$$

Equation (4-5) yields

$$a_o \simeq 16.4k^{-2.42} N_f^{-0.21}$$

$$\simeq 2.54K^{-2.42}\text{cm} \quad (1.0K^{-2.42} \text{ inches}) \qquad (4\text{-}6)$$

For a penny-shaped crack in an infinite body, $k = 2/\sqrt{\pi}$, and we obtain the unrealistically large value of $a_o \sim 1.91$ cm (0.75 inches).

It is believed that this unrealistic result is found because the strain energy in the adhesive was ignored in the analysis. This point is demonstrated in Appendix B, where the effect of the adhesive's strain energy is taken into account. It can be shown that if a correction for net section area is not made, the initial flaw size is (Equations B-12 thru B-16)

$$a_o \simeq 1.91 - a_H = 1.91 - 0.76 = 1.15 \text{ cm } (0.45 \text{ in.}).$$

If the area correction is made, and a numerical integration of Equation A-1 is performed to predict fatigue life, we find that a_o is on the order of the adhesive thickness. This prediction is sensitive to the adhesive modulus and Poisson's ratio, which are not known very accurately at this time.

Nevertheless, it is tentatively concluded that a single-stage fatigue crack growth equation, Equation (4-5), will predict the correct fatigue life if the initial flaw is a macrocrack, viz. $a_o \sim .25$ cm (0.1) in.). Futhermore, the experimental data indicates that except for the first few cycles, a_o will always be large. If the value of a_o had turned out to be much less than the bondline thickness of 0.01 inches, the number of cycles of stable microcrack growth would have to be included in the fatigue life prediction, as discussed in Appendix A. Clearly, the experimental data and analytical model are consistent and this model provides a more practical approach to lifetime prediction of the aluminum butt joints than was previously available.

5.0 ACOUSTIC EMISSION

5.1 General

Acoustic emission is a phenomenon which often occurs when solids experience a strain that is in excess of their elastic limit. The manner in which energy is released by an adhesive when subjected to load may be determined roughly from the vibrational reactions of the medium. Piezoelectric crystals provide a direct means of measuring the reactions of the adhesive by producing an analog voltage waveform representation of the deformation. These measurements generally have been restricted to counting the number of events observed, measuring event coincidence, and determining the relative maximum amplitude of the wave packet.[8,9] The purpose of the acoustic emission efforts in this program was to record and analyze the complete response of the bonded joints via real-time computer processing of the A/E data.

The fatigue of metallic structures is generally recognized as producing acoustic emission activity which can be used to characterize crack formation and propagation.[10] These events exhibit a burst type of acoustic activity which emanates from the material in the vicinity of the crack tip. Based on previous Vought studies of wedge crack opening fracture, a similar fatigue-induced acoustic behavior was expected from the adhesive system under study.

5.2 Experimental Approach

One of the major objectives of this program was to ascertain if acoustic emission and/or compliance measurement techniques could be used to detect flaw initiation and propagation in the adhesive of a bonded structure. Preliminary literature surveys revealed that most acoustic emission monitoring done to date has involved emission count to the induced strain.[11,12] It was apparent that in the present state-of-the-art a great portion of the information available is not being utilized. If Vought was to make a valid and universally accepted assessment of these techniques, an attempt must be made to evaluate every attainable data source. In particular, a concentrated effort had to be made to develop a usable and reliable source location capability.

The acoustic emission facility is based on a Trodyne six channel acoustic emission processor capable of providing all the standard data analyses. After several modifications were made to the Trodyne processor, a high speed minicomputer system was added. The following paragraphs discuss the resultant system's capabilities.

Stress caused emissions were of two general types, continuous and burst. Sources of continuous emission activity were of small magnitude, possibly created by discrete reorientation movements throughout the volume of the material. Burst emissions were created by larger, more localized activity which occurred aperiodically. A historical record was maintained of the event function, i.e., the manner in which the material emitted sound energy (continuous or burst), during each test to aid characterization of the adhesive failure mechanisms, Figure 5-1. For convenience, the results of one specimen, Aluminum Butt Joint 22 (AB-22), are presented throughout this section.

Each acoustic event arrived at the detectors as a discrete "packet" of oscillations, Figure 5-2. An order of magnitude estimate of the energy contained in the packet was obtained by examination of the amplitude of its largest oscillation. For every 100 events, the amplitude of each event's largest oscillation was averaged together and plotted as a function of time, thereby producing a record of the variation of the energy released during the test, Figure 5-3.

During the test, the A/E processor maintained a running total of the number of detected emissions. This event count was read by the computer at ten second intervals and an event rate was calculated. This information was stored and later rendered by the computer into a graphic representation which facilitated identification of periods with high emission rates, Figure 5-4.

At ten second intervals the oscillation content of an event waveform was analyzed by the A/E processor. The signal was broken into individual oscillations and each was measured to determine the distribution of the amplitudes of the oscillations over a 60 dB gain range. This data, shown in Figure 5-5, was then read by the computer and stored for later analysis.

The test specimens were instrumented with a simple geometric pattern of transducers (such as the rectangular array shown in Figure 5-6), to permit determination of the two-dimensional coordinates of the sources detected. This was done by recognizing that when an emission occurs, the sound wave propagates through the structure (assumed to be isotropic and homogeneous for this discussion) as an expanding spherical disturbance of the medium. The A/E processor measured

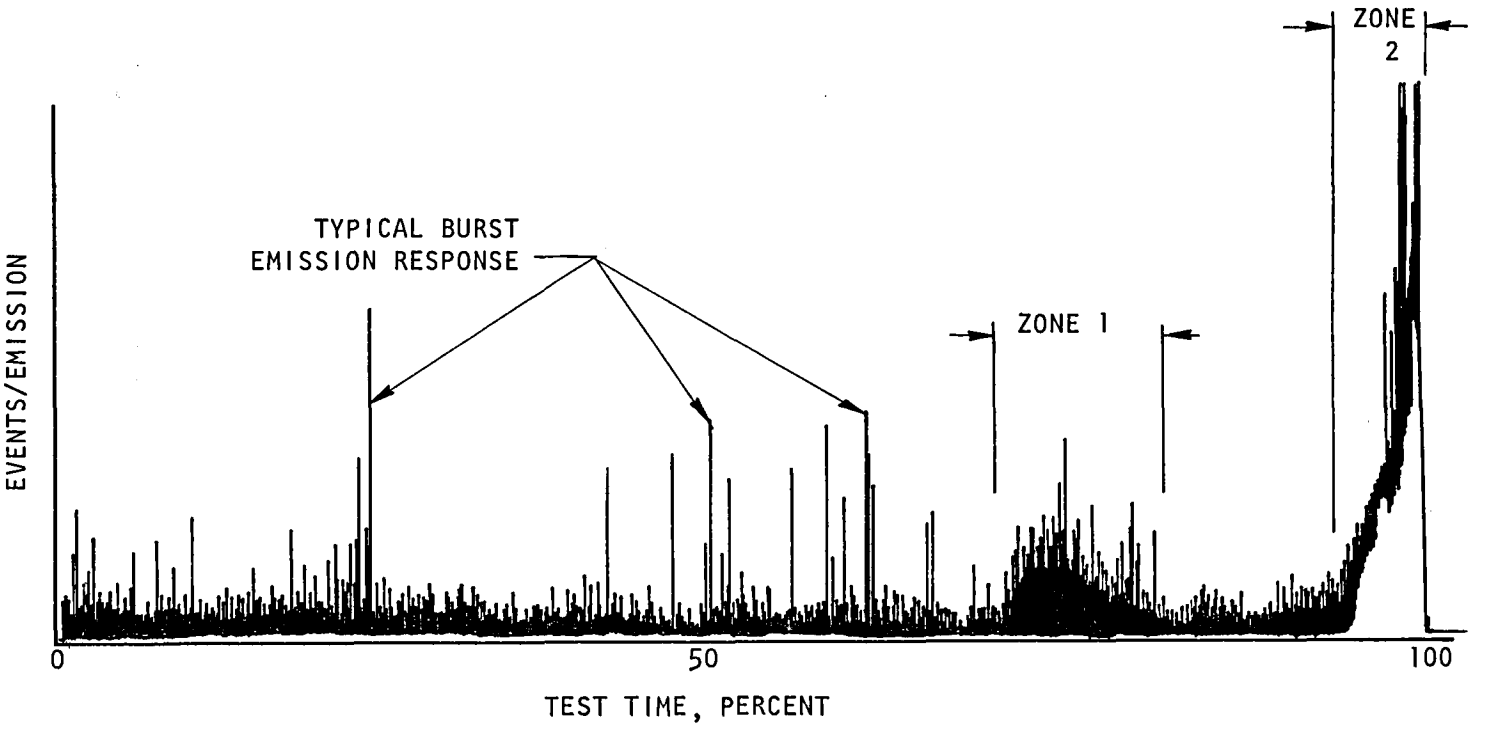

FIGURE 5-1 EVENT FUNCTION FOR ALUMINUM BUTT JOINT 22 (AB-22)

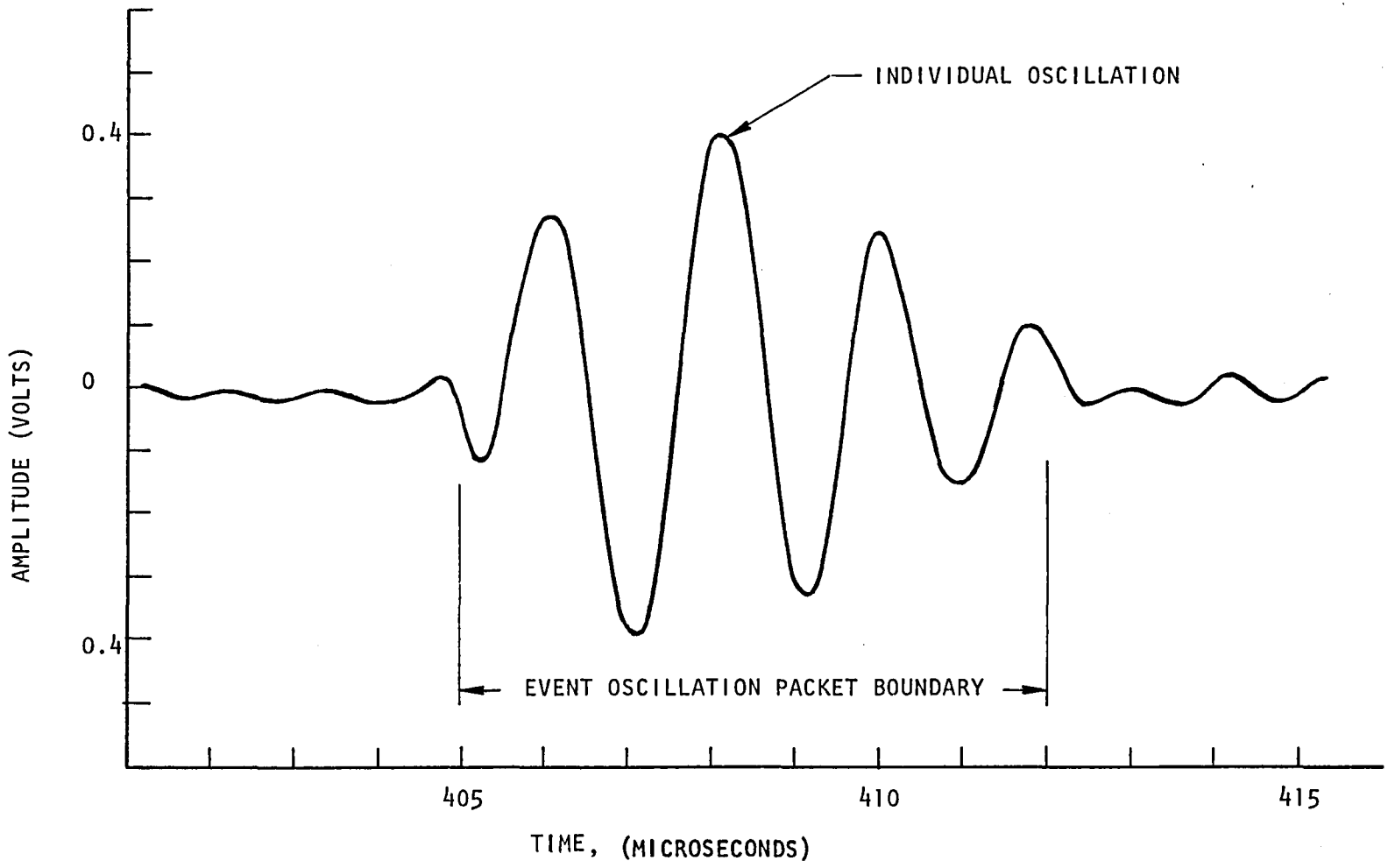

FIGURE 5-2. SAMPLE EVENT WAVEFORM

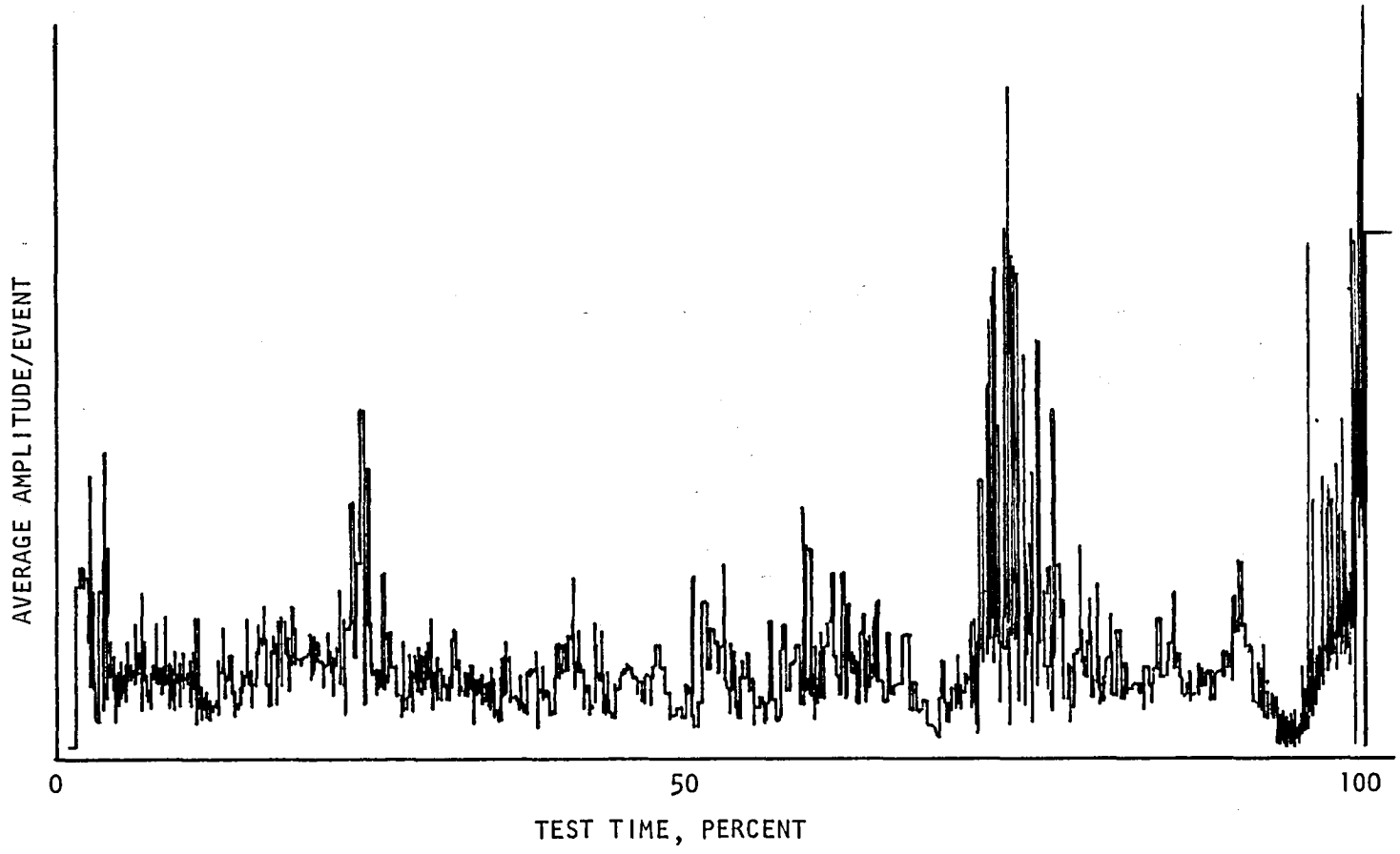

FIGURE 5-3 AVERAGE AMPLITUDE PER EVENT FOR SPECIMEN AB-22.

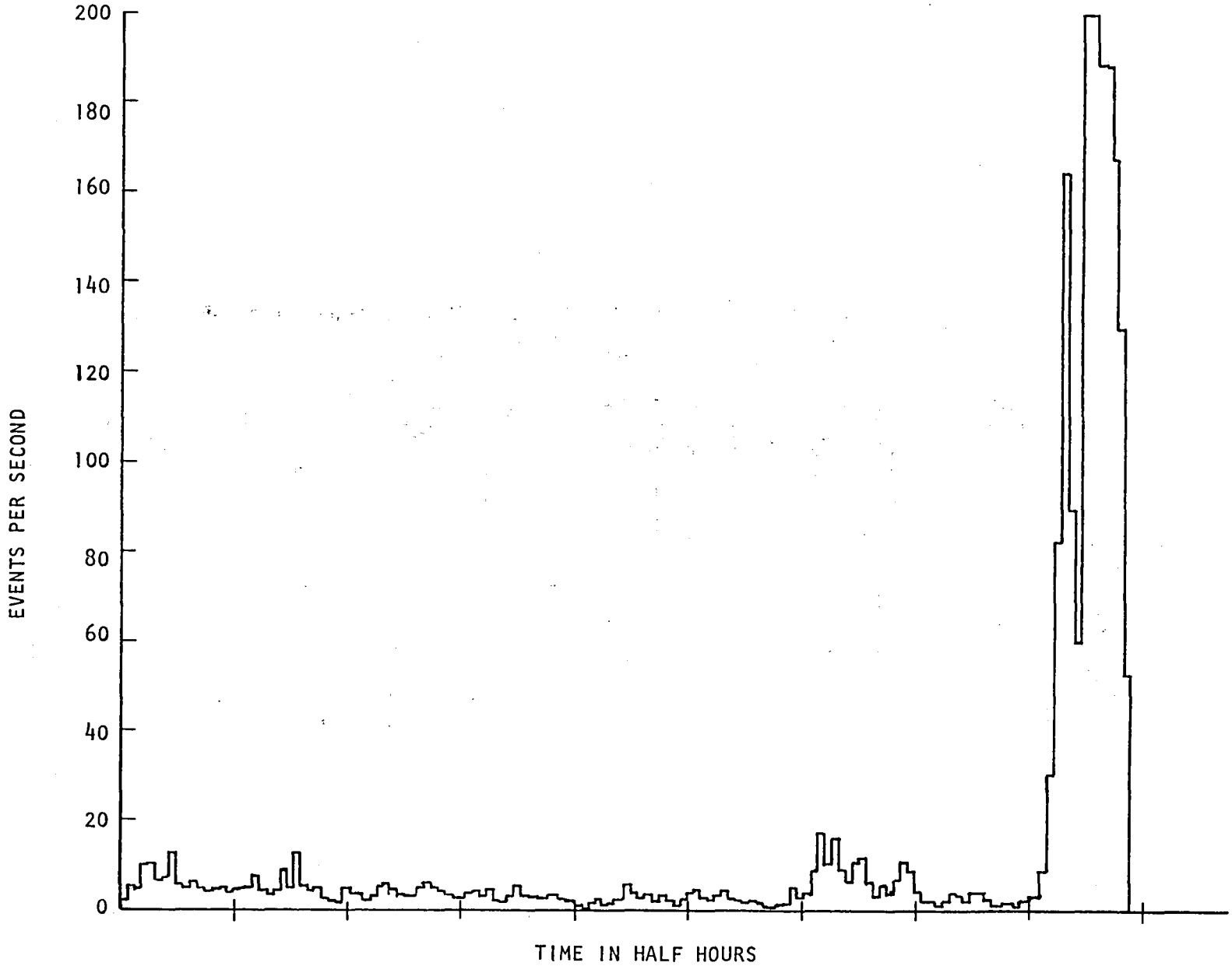

FIGURE 5-4 EVENT RATE FOR SPECIMEN AB-22

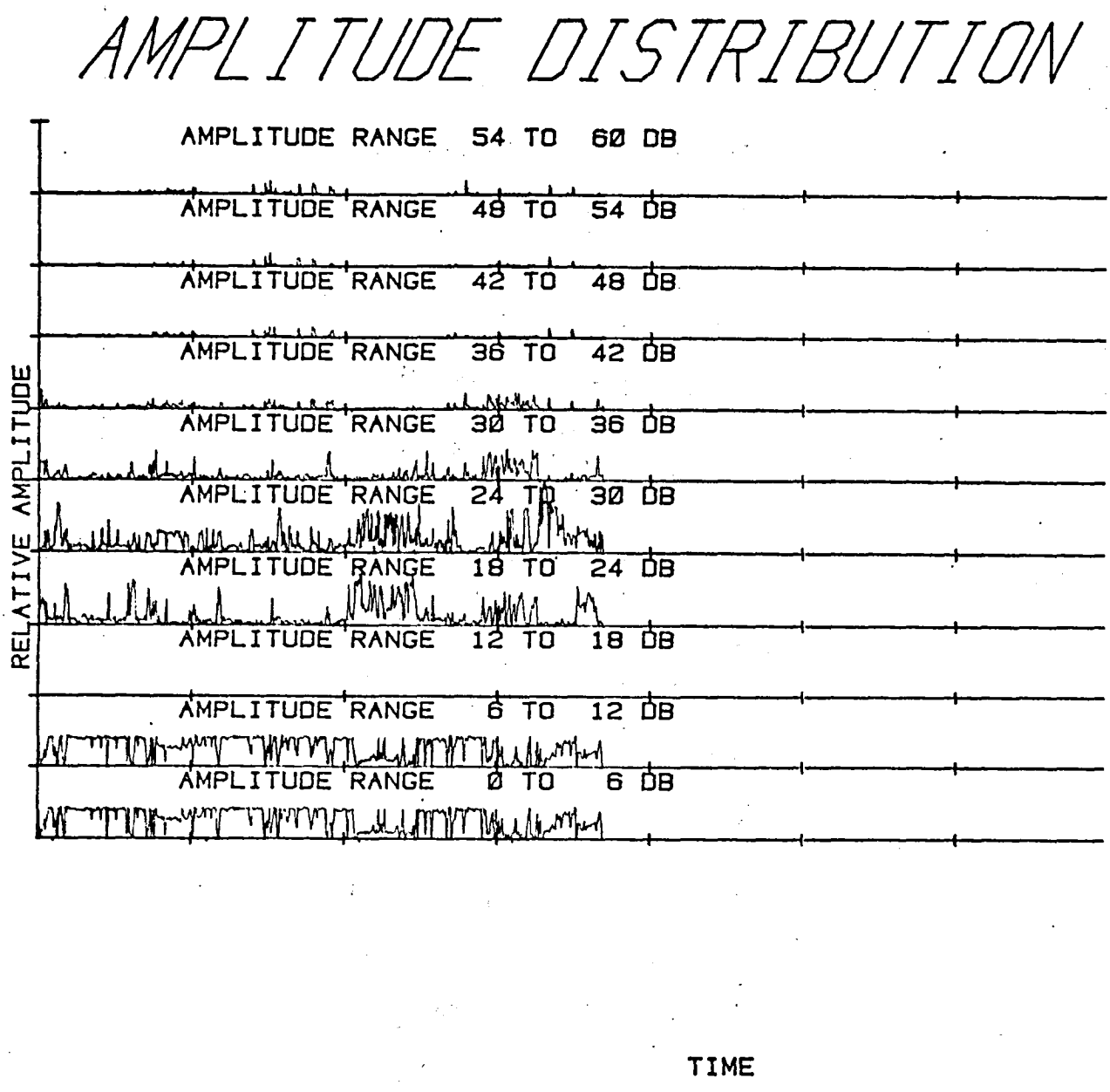

FIGURE 5-5. AMPLITUDE DISTRIBUTION FOR AB-22 IN PERCENTAGE OF ACCEPTED SIGNALS IN EACH DECIBEL RANGE

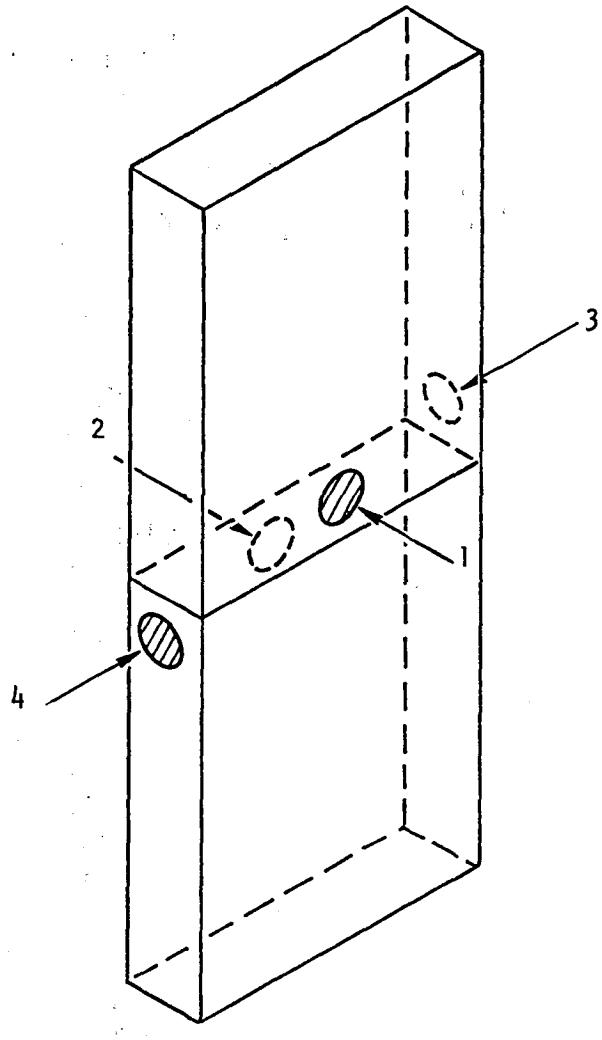

FIGURE 5-6 ULTRASONIC TRANSDUCER LOCATIONS

the differences in the times of arrival of this front at opposing transducers and then passed this information to the computer for analysis. When provided with the necessary configurational information, the computer calculated where the sound was emitted from, determined whether or not the emission was emitted from the region of interest, and determined the emission density in that area as a function of spatial location. The two-dimensional adhesive region of interest was divided into discrete "cells" whose size is a function of the uncertainty of the time difference, "Delta T", measurement and the medium. When the computer determined that the emission density in a certain cell had exceeded a preset threshold level (7% of the current sample or of the total distribution), it labeled that cell as a "special point" of acoustic emission activity and any subsequent emissions that were determined to have emanated from that cell were immediately tagged with its coordinates (in parentheses) and its time of emission, Figure 5-7.

5.3 Experimental Observations

The experimental testing was conducted at ambient temperature, pressure, and humidity. All specimens were subjected to constant amplitude fatigue at a fixed frequency. Acoustic emission monitoring was continuous as provided by the automated A/E monitoring system.

Double cantilever beam specimens were pre-cracked and then fatigued to determine one-dimensional crack growth rates in the adhesive system. The test was stopped after every 10,000 cycles so that a visual measurement of the apparent progress of the crack front could be made. When the cycling was restarted, high amplitude burst emissions were observed coming from the region immediately preceding and adjacent to (within 1.0 cm) the crack front. The real-time data presentation of the automated acoustic emission monitoring system showed that throughout the test, this activity was confined to the region of the adhesive that moved just ahead of the crack-tip. Post-test examination of the adhesive fracture surface revealed that crazing with a moderate micro-void density existed in the region which exhibited the A/E characteristics mentioned above. A cohesive failure resulted.

The general acoustic characteristics of the aluminum butt joint specimens are exemplified by those present in the data of specimen AB-22. An examination of the event function, Figure 5-1, illustrates the sequence in which the

```
SPECIAL POINT DOCUMENTATION
(  .0,-1.2)  14: 7:45
(  .0,-1.2)  14: 8:14
(  .2,-1.2)  14:10: 7
(  .0,-1.5)  14:11:25
(  .0,-1.7)  14:17:53
(  .0, 1.1)  14:21: 7
(  .2, 1.4)  14:21:42
(  .2,-1.2)  14:24:58
(  .0, 1.2)  14:25: 1
(  .0,-1.4)  14:26:47
SPECIAL POINT DOCUMENTATION
(  .2, 1.4)  15: 6:27
(  .4,-1.5)  15:11:38
(  .0, 1.8)  15:15: 1
(  .0,-1.1)  15:16: 8
(  .0, 1.5)  15:18:24
(  .0,-1.5)  15:23:12
(  .4,-1.7)  15:37: 6
(  .0,-1.8)  15:38:21
(  .2,-1.4)  15:39: 2
(  .0, 1.1)  15:39:17
SPECIAL POINT DOCUMENTATION
(  .0, 1.7)  17: 9:46
(  .0, 1.2)  17:11: 6
(  .0, 3.2)  17:12:29
(  .0, 1.2)  17:12:39
(  .0, 2.3)  17:13:29
(  .6, 1.2)  17:13:35
(  .2, 1.4)  17:14:38
(  .2, 1.7)  17:20:32
(  .0, 1.2)  17:20:53
(  .5, 1.8)  17:25:40
```

FIGURE 5-7. SPECIAL POINT DOCUMENTATION OF AB-22. COORDINATES (IN CENTIMETERS) APPEAR IN PARENTHESES AND TIME OF EMISSION IN HOURS:MINUTES:SECONDS.

emissions arrived at the sensor (burst or continuous mode), as opposed to the rate that they arrived. The vertical scale gives an indication of the number of events that arrived in each pulse or burst. Note that, with only a few minor exceptions, the first 85% or so of the test can be characterized by burst emission; that is to say that a number of events arrived at the sensor within a very short time interval, then there was a period in which no events were detected, and the process continued. There was a region (Zone I) of burst emission activity which began about 65% and extended to about 75% of the specimen lifetime. It is interesting to note the elevated intensity of the burst emissions of this zone and their close proximity to each other. Another region of interest in Figure 5-1 (Zone II) began around 90% of the test and continued through failure. This region exhibited a pronounced continuous emission as demonstrated by the plot baseline rarely returning to the abscissa.

There was a distinct difference between the event function, shown in Figure 5-1, and the actual event rate, shown in Figure 5-4. Note that the areas corresponding to Zones I and II are clearly distinguishable due to the elevation of their respective rates above the background level. The emission event rate for Zone I was on the order of 10 to 20 events/second and the rate for Zone II was substantially higher and approaches 200 events/second. It should also be noted that the average amplitude per event function (Figure 5-5) not only was on the same order of magnitude but appeared comparable in every respect.

The source location information presented in Figure 5-8 is a graphic representation of the bond area generated by the computer about 25% of the way through the test. Figure 5-12 is a photograph of the failed adhesive surface (the axes drawn on the surface correspond to the axes in the computer graphic). The computer graphic (Figure 5-8) shows the total number of discrete events that have accumulated up to that point in time in a corresponding area inside the bondline, since the beginning of the test. (The negative signs which precede some of the data values are flags generated by the computer which label those particular locations as "special points" of high accumulated acoustic activity.) This figure shows that the highest density of source locations in the adhesive is an elliptical region centered slightly above the origin, which is the same area that has the most crazing and the highest micro-void density on the failed surface. Figures 5-9, 5-10, and 5-11 are similar computer graphic

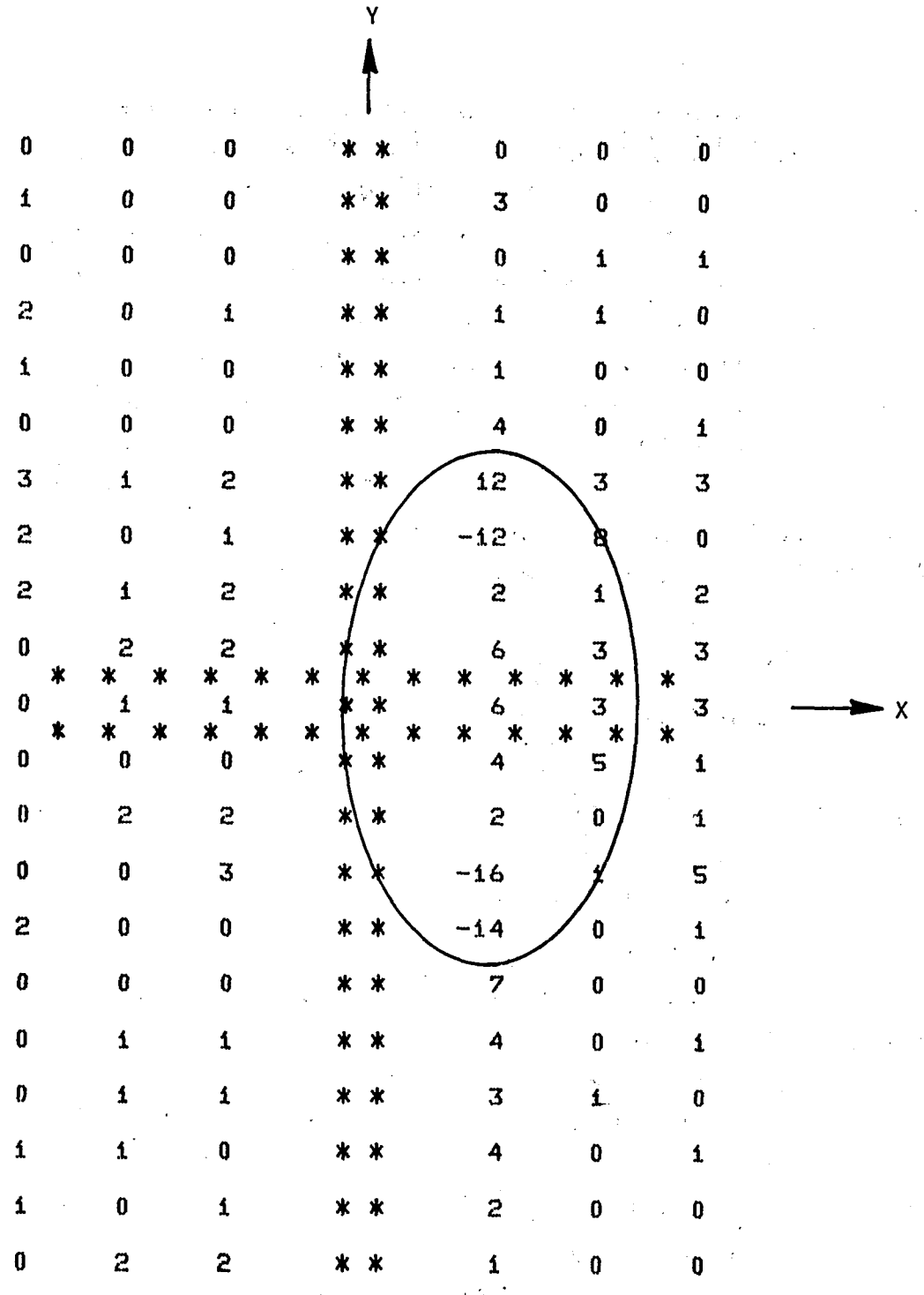

FIGURE 5-8. CUMULATIVE SOURCE DISTRIBUTION FOR AB-22 AFTER 200 SOURCES. FILE CLOSED AT 14:24:58.

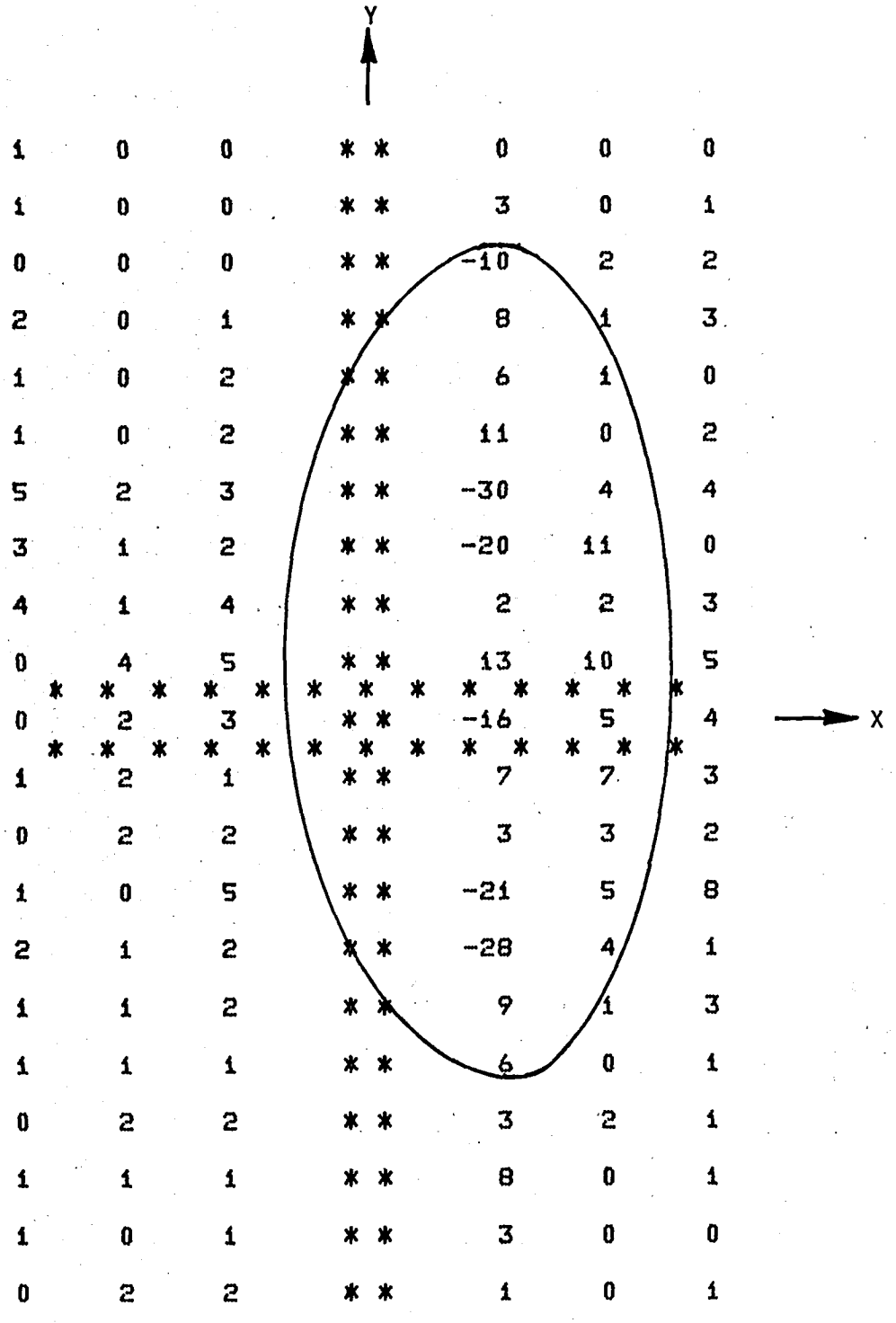

FIGURE 5-9. CUMULATIVE SOURCE DISTRIBUTION FOR AB-22 AFTER 400 SOURCES. FILE CLOSED AT 15:45:28.

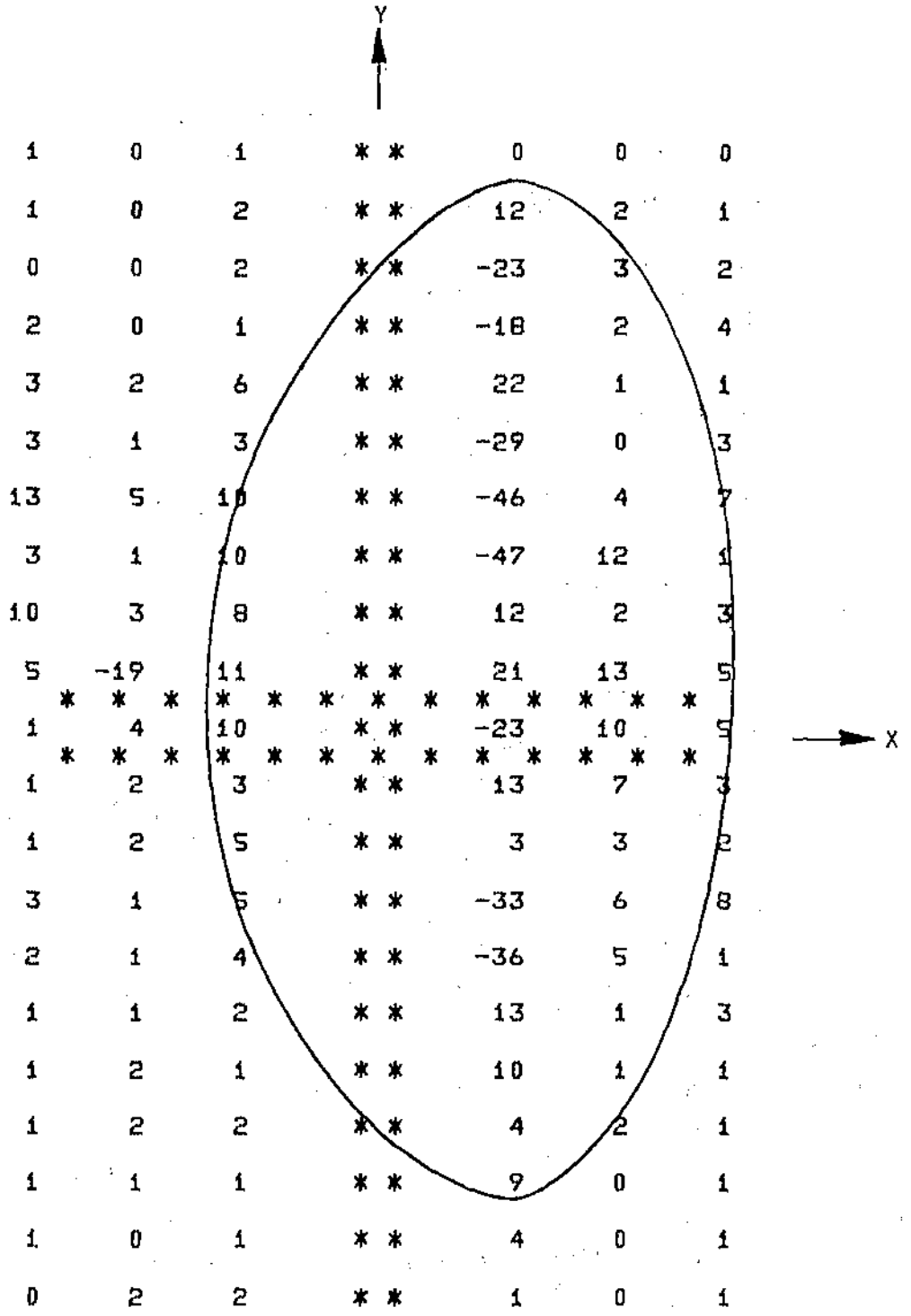

FIGURE 5-10. CUMULATIVE SOURCE DISTRIBUTION FOR AB-22 AFTER 700 SOURCES. FILE CLOSED AT 16:51:08.

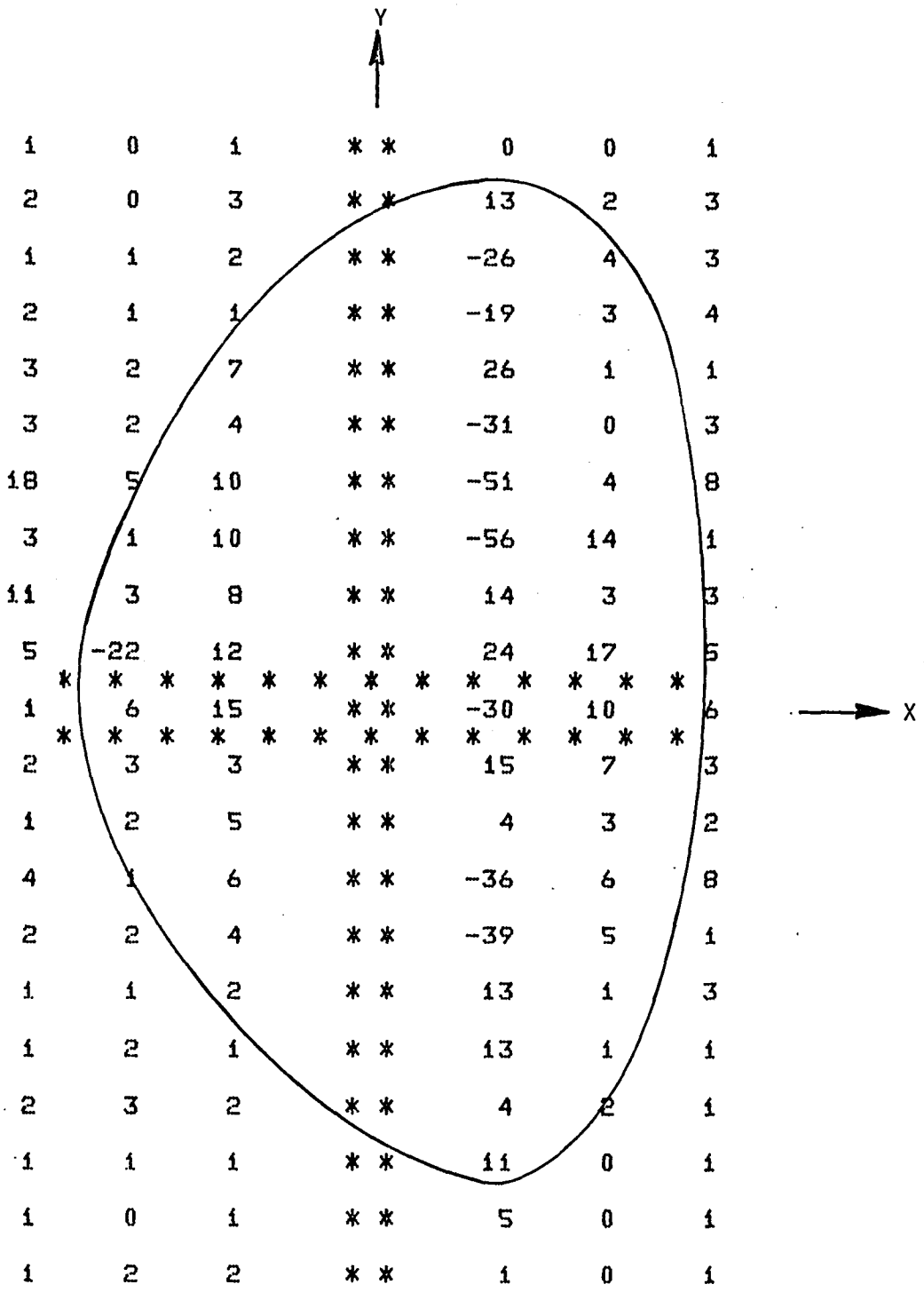

FIGURE 5-11. CUMULATIVE SOURCE DISTRIBUTION FOR AB-22 AFTER 800 SOURCES. FILE CLOSED AT 17:49:26.

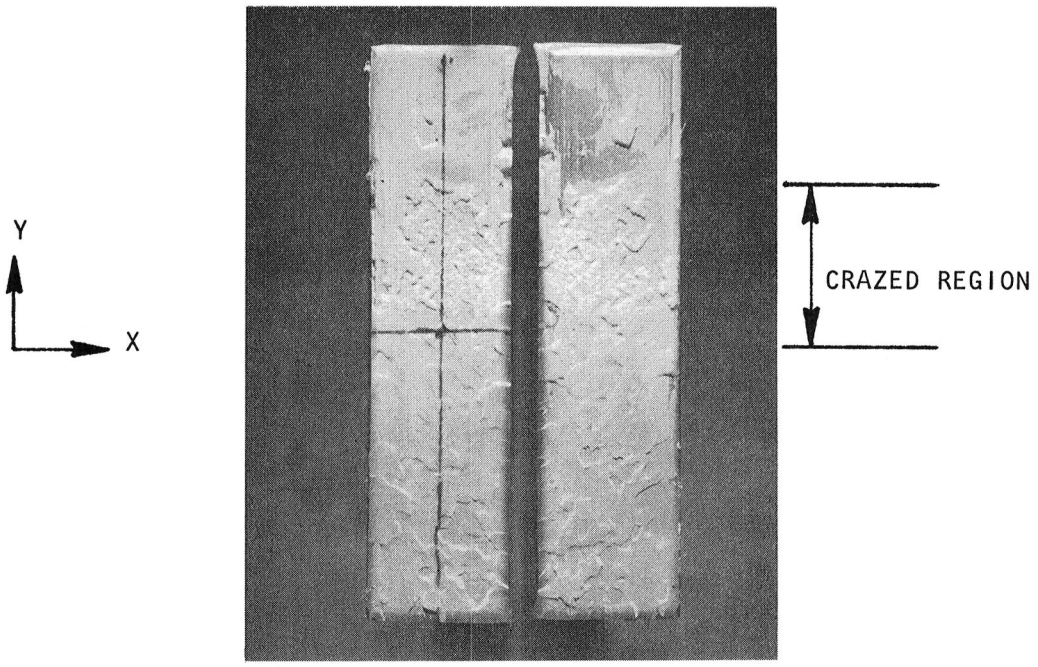

FIGURE 5-12. FRACTURE SURFACE OF SPECIMEN AB-22 SHOWING ACOUSTIC AXES AND CRAZED REGION

outputs which were obtained at approximately 50%, 75%, and 100% of the way through the test of AB-22, respectively. The similarity of these figures is important. The region of high density remains, effectively, the same size; only the degree of emission density increases from one to the other. In particular, the rate at which the emissions occurred that actually emanated from the respective regions of the bond appears to be fairly uniform with time. Two-hundred discrete source locations comprise the listing taken at 25%. Two-hundred new sources are present in the listing taken at 50%, three-hundred more in the listing taken at 75%, and only one-hundred new sources were added during the final interval before failure.

It is apparent from the foregoing discussion that Zone I produced three times the number of valid source locations as did Zone II, even though the total number of emissions in Zone II was at least two orders of magnitude greater than that in Zone I based on an analysis of Figure 5-4. This type of signature was present in the majority of aluminum butt-joint specimens which were found to be relatively free of adhesive defects. The occurrence of the type of activity demonstrated by that shown in Zone I was observed to initiate in the majority of the specimens at 55% of the fatigue life (plus or minus 10%), and the activity exemplified by that shown in Zone II was observed to begin at 90% of the fatigue life (plus or minus 5%).

Acoustic emission monitoring of the aluminum scarf and graphite/epoxy butt joints was less definitive. The adhesive material in these joint configurations was not acoustically active enough to provide sufficient documentation of adhesive degradation.

6.0 DISCUSSION & CONCLUSIONS

The purpose of this program was to assess the ability of a linear elastic fatigue failure theory to predict failure of an adhesive in a primary bonded composite structure. The use of acoustic emission and/or compliance measurement techniques was proposed as state-of-the-art methodology in attempting to detect flaw initiation and growth. This 13-month exploratory research program provided the following conclusions:

- o A fatigue failure theory was developed that was found applicable to aluminum butt joint fatigue life prediction.
- o A failure mechanism other than that seen in the aluminum joints dominates the failure of graphite/epoxy butt joints as seen in the acoustic, visual, and theoretical interpretations of the data. Yet, the generalized failure theory for aluminum butt joints is thought to be extendable to composite adherend joints.
- o The combined normal and shear stress states inherent in a scarf joint configuration cause a significantly different failure mechanism which may require an alteration in the fatigue theory due to the theory's Mode I derivation.
- o The aluminum scarf joints show the most consistency in test results, but the number of specimens tested did not provide an adequate statistical base to accurately assess the theory.
- o Acoustic emission monitoring techniques can provide reliable information concerning microvoid formation fatigue failure of adhesives. This is evidenced by the correlation of acoustic emission and post-test failure surface examination of the aluminum and graphite/epoxy butt joint specimens.
- o The compliance measurement response offered no additional information as to the mechanisms of failure which occurred in any of the specimen geometries.

The primary difference between the aluminum and graphite/epoxy butt joints appeared to be in their sensitivity to initial edge flaws and the stress concentrations occurring in the corners and on the sides of the bondline. Whereas the aluminum joints allowed the development and propagation of weakened area

within the bondline, the graphite/epoxy edge stress concentrations were large enough to cause failure before internal damage had a chance to develop. This flaw sensitivity is seen also in the large scatter in the measured fatigue lifetime of the graphite/epoxy butts.

Acoustic emission monitoring identified a repeatable pattern of regions in the aluminum butt lifetime corresponding to high amplitude/burst (at 55% of fatigue life) and high amplitude/continuous (at 90% of fatigue life) emissions. These regions or zones occurred at the same percent total life for each aluminum butt joint tested $\pm$5%. In a parallel IR&D effort several attempts were made to generate software that would capture and analyze a digital representation of individual acoustic emission waveforms. Preliminary analysis indicated that with further development work it would be possible to relate specific events with waveform parameters and thus provide a significant increase in the accuracy and reliability of this technique.

The results of this program show that the fatigue failure of similar aluminum and graphite/epoxy joints indeed occur due to different mechanisms, i.e., understanding the behavior of an aluminum joint may not offer any significant clue to the failure mechanism in a like graphite/epoxy joint. With the very real possibility of the next generation of aircraft structure being primarily composite oriented, a need exists to identify, quantify and predict the failure of composite material primary bonded structure in all temperature and moisture environments. Therefore, further study is recommended which addresses the failure of single lap, double lap, scarf and stepped lap joints with graphite/epoxy as well as graphite/epoxy-aluminum adherend combinations to model state-of-the-art bonded joint design. Emphasis should be placed on basic understanding of fatigue failure mechanisms and the applicability of accelerated testing techniques.

7.0 SUMMARY

Through the investigation of the fatigue response of several different adhesive joint configurations, the power law crack growth relationship was found to accurately model the (aluminum butt) joint lifetime. The observed failure mode of the bond was: growth of initial microscopic voids in the presence of applied stress; coalescence of these voids forming a localized weakened area and growth of this weakened area; catastrophic failure of the adhesive joint. The extent of the weakened area was apparent on the failed surface due to its stress-whitened (crazed) region. Although this region was present on all failure surfaces, the character of the crazing as well as the failure surface topography varied between specimen configurations.

Post-test visual inspection of the bondline showed that the size and location of craze formation corresponds with the results obtained through the use of automated acoustic emission monitoring techniques. The general characteristics of the acoustic emission signals (i.e., event rate, event function and average amplitude) and their times of occurrence have shown to be repeatable between (aluminum butt joint) specimens to an accuracy of $\pm 5\%$ of the total fatigue lifetime. All experimental measurements were made in customary (English) units and converted to S.I. units for the purposes of this report.

On the basis of these results, further investigation is needed into the failure mechanism of the scarf and graphite/epoxy butt joint, to fully understand the subtleties of these particular failure processes.

REFERENCES

1. Dance, W. E. and Petersen, D. H., "Verification of the Structural Integrity of Skin-to-Spar Adhesive Bondlines by Neutron Radiography," Journal of Applied Polymer Science, 32, pp. 399-410, 1977.

2. Damage Tolerant Design Handbook, MCIC-HB-01, Part 2, January 1975, page 11.1.3-4.

3. Mostovoy, S., Bersch, C. F., Ripling, E. J., "Fracture Toughness of Adhesive Joints," SAMPE Conference, October 1970, page 273.

4. Hertzberg, R. W., Manson, J. A., and Wu, W. C., "Fracture of Polymers and Fatigue Crack Propagation," STP 536, August 1972.

5. Renton, W. J., "Analysis and Design of Adhesive Mechanical Characterization Test Specimens," The Journal of Adhesion, Volume 10, Number 2, 1979.

6. Brussat, T. R. and Chiu, S. T., "Fracture Mechanics for Structural Adhesive Bonds - Final Report," AFML-TR-77-163, October 1977.

7. Halpin, J. C., Jerina, K. L., and Johnson, T. A., "Characterization of Composites for the Purpose of Reliability Evaluation," Analysis of Test Methods for High Modulus Fibers and Composites, ASTM STP 521, 1973, p. 5.

8. Bailey, C. D., Hamilton, J. M. and Pless, W. M., "A/E Monitoring of Rapid Crack Growth in a Production Size Wing Fatigue Test Article," NDI International, December 1976.

9. Brockman, I. W. and Fischer, T., "Acoustic Emission as a Method of Testing Adhesive Metal Joints," presented at the 22nd National SAMPE Symposium and Exhibition, San Diego, April 1977.

10. Harris, D. O. and Dunegan, H. L., "Continuous Monitoring of Fatigue Crack Growth by Acoustic Emission Techniques," Experimental Mechanics, Volume 14, 1974.

11. Soffel, A. R., "Acoustic Emission Testing of the Lance Missile Structure," ATC Report B-94100/1TR-20, Vought Corporation Advanced Technology Center, August 1972.

12. Henneke II, E. G., Jones, G. L., Herakovich, C. T., and Renieri, M. P., "Acoustic Emission from Composite Reinforced Metals, Experimental Mechanics, Volume 15, June 1975.

13. Manson, S. S., Freche, J. C. and Ensign, C. R., "Application of a Double Linear Damage Rule to Cumulative Fatigue," ASTM STP 415, 1967, p. 384.

14. Renton, W. J. and Vinson, J. R., "Fatigue Response of Anisotropic Adherend Bonded Joints," presented at AMMRC Symposium on Solid Mechanics, 1974: The Role of Mechanics in Design - Structural Joints, September 1974.

15. Schapery, R. A., "Deformation and Failure Analysis of Viscoelastic Composite Materials," Proceedings of ASME National Meeting, Special Session of Inelastic Behavior of Composite Materials, November 1975, p. 127.

16. Schapery, R. A., "Application of Viscoelastic Fracture Mechanics to Nonlinear Behavior and Fracture of Solid Propellants," Texas A&M Research Report MM 2995-74-5, July 1974.

17. "Definition and Non-Destructive Detection of Critical Adhesive Bond-Line Fibers," AFML-TR-78-108, July 1978.

18. Rabinowitz, S. and Beardmore, P., "Cyclic Deformation and Fracture of Polymers," Journal of Material Science, Volume 9, 1974, pp. 81-99.

19. Schapery, R. A., "A Theory of Crack Initiation and Growth in Viscoelastic Media, III. Analysis of Continuous Growth," International Journal of Fracture, Volume 11, No. 4, August 1975, pp. 549-562.

20. Manson, J. A. and Sperling, L. H., Polymer Blends and Composites, Plenum Press, New York, 1976.

21. Mostovoy. Sheldon and Ripling, E. J., "Fracturing Characteristics of Adhesive Joints," Final Report Contract No. N00019-73-C-0163, January 31, 1974.

22. Broek, D.,Elementary Engineering Fracture Mechanics, Noordhoff, 1974 (Chapter 5).

23. Sih, G.C.,(Editor), Method of Analysis and Solutions of Crack Problems, Noordhoff, 1973, pp. 357-8.

24. Fourney, M. E., Muki, R., Stone, S. F., and Westmann, R. A., "Role of Bond Thickness on Adhesive Failure," Polymer Engineering and Science, Vol. 19, No. 2, pp. 114-117, 1979.

25. Arin, K. and Erdogan, F., "Penny-Shaped Crack in an Elastic Layer Bonded to Dissimilar Half Spaces," International Journal of Engineering Science, Vol. 9, pp. 213-232, 1971.

26. Erdogan, F. and Gupta, G., "The Stress Analysis of Multi-Layered Composites with a Flaw," International Journal of Solids and Structures, Vol. 7, pp. 39-61, 1971.

APPENDIX A

FATIGUE FAILURE THEORY

Numerous fatigue failure theories are available which attempt to describe the fatigue failure mechanisms in metal structures. Among these are Miner's Rule and the Double Linear Damage Rule proposed by Manson, Freche and Ensign.[13] Attempts to formulate a fatigue failure criterion for adhesives appear to be absent from the published literature, except for an initial attempt by Renton and Vinson.[14] Such a theory, to possess a high probability for success, must analytically relate this criterion to the viscoelastic and fatigue crack growth response of the adhesive. Review of the literature reveals that a theory proposed by Schapery[15] incorporates these effects for viscoelastic polymers. Its limited use with propellant[16] and fibrous composite materials[15] is encouraging. Therefore, use of this fundamental theory to formulate a fatigue failure criterion for adhesives is made here.

Stable and Unstable Growth of Cracks

Development of a fatigue failure criterion is aided by first studying the opening-mode propagation behavior of a single planar crack. For this study, crack speed, expressed as the amount of crack growth per cycle, da/dN, was assumed to obey a power law in terms of the amplitude of the stress intensity factor,

$$\frac{da}{dN} = c(\Delta K_I)^q \qquad \text{(A-1)}$$

where q is a positive constant. This equation is based on a large amount of fatigue data for polymers subjected to fatigue loading at constant frequency η, temperature T, and R-value.[15,6] The coefficient c can be expected to depend on these three parameters as well as the number of cycles, N, through the effect of cycling on the softening of the material in which the crack propagates.[15] However, the exponent q does not seem to vary, at least over a limited range of loading and environmental conditions.[15,6]

For an isolated, penny-shaped crack

$$\Delta K_I = k\sqrt{a}\,\Delta\sigma \qquad \text{(A-2)}$$

where $k = 2/\sqrt{\pi} \simeq 1.13$, a = crack radius, and $\Delta\sigma$ = remote tensile stress amplitude. When the crack is not isolated (e.g., interaction with boundaries or other cracks exists) and is not circular, the factor k will usually vary in

time; we have allowed for such possibilities in this analysis.

Now, without restricting c and k to be constants, we calculate the instantaneous size a by substituting Eq. (A-2) into (A-1) and integrating,

$$a = a_o(1 - p\, a_o^p\, I_N)^{-1/p} \tag{A-3}$$

where

$$p \equiv \frac{q}{2} - 1 \tag{A-4}$$

$$I_N \equiv \int_o^N ck^q(\Delta\sigma)^q\, dN \tag{A-5}$$

and a_o is the initial crack size. Observe that $a \to \infty$ when $I_N \to (pa_o^p)^{-1}$, which can be interpreted as failure, i.e., neglecting inertia, the crack becomes unstable at the critical value,

$$I_f \equiv (p\, a_o^p)^{-1} \tag{A-6}$$

This result defines the fatigue life N_f through Eq. (A-5),

$$\int_o^{N_f} ck^q(\Delta\sigma)^q\, dN = (p\, a_o^p)^{-1} \tag{A-7}$$

It should be noted that these observations on failure require that $q > 2$ (Eq. (A-4)) and that c, k, and $\Delta\sigma$ not diminish rapidly with N; if the integrand in Eq. (A-5), $ck^q(\Delta\sigma)^q$, decreases sufficiently fast with N, the value of I_f will not be reached regardless of how many cycles are applied. Such behavior could result due to energy absorption mechanisms in the crack plane or from changes in bondline thickness incorporated to reduce the stress intensity factor for adhesive flaws.

In order to illustrate the behavior predicted by Eq. (A-3) it is helpful to first introduce Eq. (A-6) and obtain

$$\frac{a}{a_o} = \left(1 - \frac{I_N}{I_f}\right)^{-2/(q-2)} \tag{A-8}$$

which is plotted in Figure A-1 for $q = 6$ and 12. I_N/I_f could be interpreted as a damage ratio in that when $I_N = I_f (I_N/I_f = 1)$ failure occurs. Note that if c, k, and $\Delta\sigma$ are constant,

$$\frac{I_N}{I_f} = \frac{N}{N_f} \tag{A-9}$$

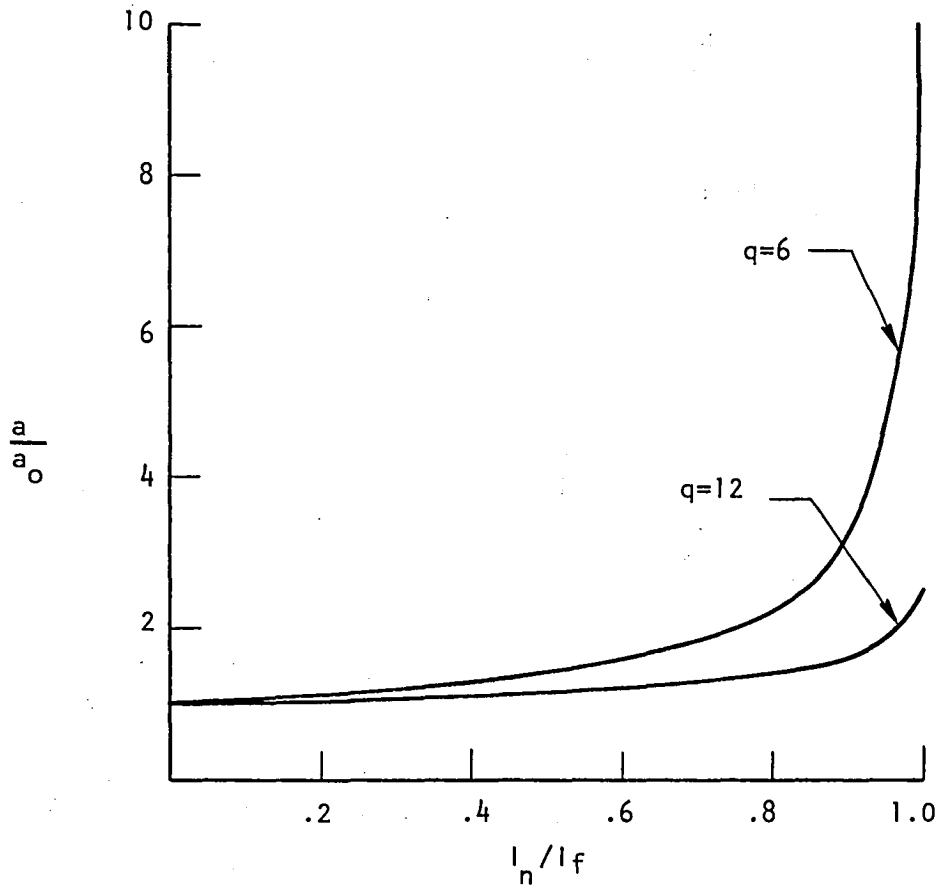

FIGURE A-1 RELATIVE AMOUNT OF CRACK GROWTH AS A FUNCTION OF DAMAGE RATIO.

which is the proportion of the fatigue life that has been used after N cycles. The crack size at 90% of the life ($N = .9\ N_f$) is found from Eq. (A-8) to be

$$\frac{a}{a_o} = 10^{1/P} = 10^{2/(q-2)} \tag{A-10}$$

For example, if $a = 3.2\ a_o$ when $q = 6$ and $a = 1.6\ a_o$ when $q = 12$ then most of the life would be used up before the crack undergoes much growth.

The latter observation of this example is very important as it implies that an initially isolated flaw will remain isolated during most of its life. (This conclusion depends on q being relatively large and the integrand in Eq. (A-5) being constant or, if not, at least not decreasing significantly in time; both conditions are often met in practice.) A key result is that the fatigue life, therefore, can be estimated in many cases without having to account for interactions with other cracks or boundaries. It should be added that these interactions may be accounted for in principle through the factor k; for example, k would diminish with crack growth if a barrier is encountered such as a spherical void in an adhesive layer which could blunt a crack or the microparticles in the case of elastomeric-modified adhesives.

A Stochastic Model For Fatigue Failure

We now consider a universe of specimens (i.e., adhesive layers) which are identical except for the distribution of initial flaws. It is assumed that the failure process can be modeled by means of Eq. (A-7) in that global failure is the result of a dominant crack in each specimen becoming unstable. Interactions with other cracks during stable growth is not precluded at this point in the development of the model.

The initial size of the "dominant crack" in the ith specimen is denoted by a_{oi}. The "dominant crack" is the one crack which ultimately leads to fracture. Variations of the values of c and k from specimen to specimen were taken into account in this analysis, but we did assume that any change with time is the same for all specimens; vis., for the dominant crack in the ith specimen,

$$\begin{aligned} c_i &= c_{oi}\ C \\ k_i &= k_{oi}\ K \end{aligned} \tag{A-11}$$

where the subscript "o" indicates an initial value. According to Eq. (A-7) the ith specimen fails at $N = N_{fi}$, where

$$\int_{o}^{N_{fi}} C\, K^{q}\, (\Delta\sigma)^{q}\, dN = e^{F_i}. \qquad \text{(A-12)}$$

By definition,

$$e^{F_i} \equiv (p\, a_{oi}^{P}\, c_{oi}\, k_{oi}^{q})^{-1} \qquad \text{(A-13)}$$

The parameter F_i is introduced through an exponential relation in order to simplify later considerations of experimental data. It is seen that the effect of separate statistical distributions of a_o, c_o, and k_o on failure is through a single statistically distributed parameter, F.

Denoting the frequency distribution of F by $P_F = P_F(F)$, $P_F dF$ is the proportion of specimens having F values between F and F + dF. Inasmuch as the integrand in Eq. (A-12) is positive and the index "i" appears on only N and F, this relation implies only one value of N is associated with each value of F. Therefore, with $P_N \equiv P(N)$ denoting the frequency distribution of fatigue lifes, N, it follows that

$$P_N\, dN = P_F\, dF\ . \qquad \text{(A-14)}$$

The proportion of specimens which fail between N = 0 cycles and $N = N_T$ cycles is equal to the integral of P_N over this range. This implies, therefore, that the probability of failure occurring during N_T cycles is

$$P_f\ (0 \leq N \leq N_T) = \int_{o}^{F_T} P_F\, dF \qquad \text{(A-15)}$$

where, from Eq. (A-12),

$$F = \ln\left[\int_{o}^{N} CK^{q}(\Delta\sigma)^{q}\, dN\right] \qquad \text{(A-16)}$$

Also, $F_T \equiv F(N_T)$; i.e., F_T is the value of F at the number of cycles N_T.

Equation (A-15) is valid for constant and variable amplitude and frequency loading under constant or transient temperatures (assuming, of course, the crack growth model applies to all these conditions). However, before we can apply this failure probability prediction technique, the distribution function P_F and the parameters C, K, and q have to be established from our experimentation. We shall discuss here the experimental determination for the case in which C = K = 1, implying from Eq. (A-11) that c and k are constant during

the fatigue tests. With this limitation, the only experimentation needed was constant amplitude fatigue tests. Equation (A-16) becomes

$$F = \ln N + q \ln \Delta\sigma \ . \qquad \text{(A-17)}$$

In view of Eqs. (A-15) and (A-17), the cumulative distribution functions for different stress amplitudes illustrated in Figure A-2 are identical in shape, and differ only with respect to their location on the ln N axis.

Thus, assuming the model is valid for all cases, one can obtain statistical data at different amplitudes (say $\Delta\sigma_j$) and then form a "master" cumulative distribution function by graphically translating the data to a reference curve (say $\Delta\sigma_1$). If the value of q is not known a priori, it can be found from the amount of translation required. The derivative of the master curve with respect to ln N is simply the function P_L. This procedure permits one to establish P_L with a relatively small number of tests at each stress amplitude, especially if q is already known for the particular adhesive of interest. In this latter case, we can simplify the application of this analysis by introducing a "reduced life" parameter, $\tilde{N}_j$, for the ith amplitude,

$$\tilde{N}_j \equiv \left(\frac{\Delta\sigma_j}{\Delta\sigma_1}\right)^q N \ . \qquad \text{(A-18)}$$

Then one can construct directly a master cumulative distribution function by plotting cumulative failure data against $\tilde{N}_j$ or $\ln \tilde{N}_j$.

Analysis For Multiple Stages of Crack Growth

The basic relation for crack growth, Eq. (A-3), is potentially applicable to microcrack growth (small crack relative to bondline thickness) and to subsequent macrocrack growth (large crack relative to bondline thickness). In order to clarify this point, let us first suppose that q is the same for both types of cracks. Then we apply Eqs. (A-3)-(A-5) to the crack that is ultimately responsible for specimen failure, that is, the "dominant" crack. The integral I_N, Eq. (A-5), may be written as

$$I_N = I_N(N) = \int_o^{N_1} c_1 k_1^q (\Delta\sigma)^q \, dN + \int_{N_1}^{N} c_2 k_2^q (\Delta\sigma)^q \, dN \qquad \text{(A-19)}$$

where N_1 is the microcrack fatigue life in that the difference $[1 - p\, a_o^p I_N(N_1)]$, although not zero, is extremely small. The coefficient $c_1 k_1^q$ is that for a microcrack and $c_2 k_2^q$ is for a macrocrack. If these two coefficients are

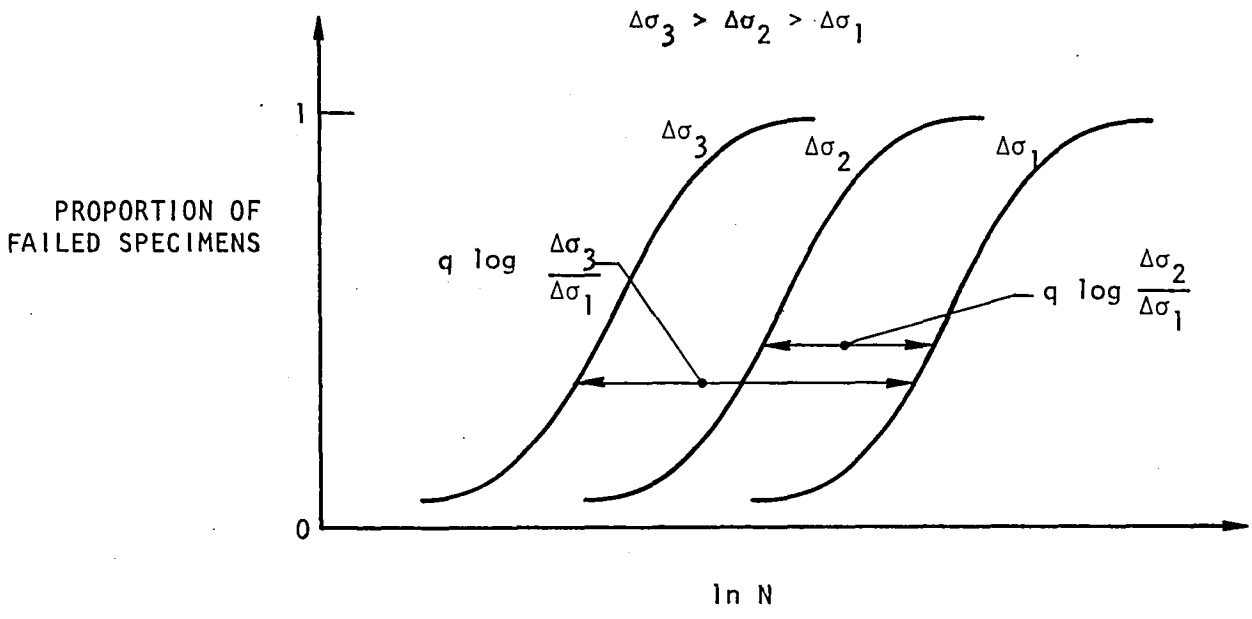

FIGURE A-2 CUMULATIVE DISTRIBUTION FUNCTIONS FOR FATIGUE LIFE

comparable in magnitude then the macrocrack life $N_f - N_1$ may be neglected relative to the microcrack life, N_1, and thus $N_f \simeq N_1$. However, if $c_2 k_2^q$ is relatively much smaller it may be true that $N_f - N_1 >> N_1$; viz., $N_1 \simeq 0$ and only the second integral in Eq. (A-19) needs to be used in calculating fatigue life. It should be noted that c_1 reflects the very small scale local adhesive mechanical properties and fracture energy, and c_2 the large scale, "effective" mechanical properties and fracture energy. With the above interpretations and idealizations, Eq. (A-15) applies to the two-stage growth process in which

$$F = \log\left[\int_o^{N_1} C_1 K_1^q (\Delta\sigma)^q \, dN + \int_{N_1}^{N} C_2 K_2^q (\Delta\sigma)^q \, dN\right] . \qquad \text{(A-20)}$$

On the other hand, the value of q may be different for microcracks and macrocracks. For this situation Eq. (A-7) would be used to predict the microcrack life $N_f = N_1$, and through Eq. (A-15) the distribution of microcrack lives. The macrocrack life and distribution of lives would be predicted by means of the same equations, except a_o would be interpreted as the initial macrocrack size; also, the function P_F may be different for the two scales of cracks. The total fatigue life is the sum of the lives for each scale of growth. If the "initial" macrocrack results from a process other than that of crack growth, the appropriate equations for the process would have to be used to predict the microflaw life unless, of course, this life is negligible relative to the macrocrack life. As noted elsewhere in this report, experimental evidence obtained for the particular adhesive studied on this project seems to indicate the microflaw is essentially a spherical cavity which undergoes unstable (rapid) growth at N_1, and that this microflaw life is small relative to the total fatigue life.

Effect of Temperature On Fatigue Life

The temperature can affect the life through its influence on the basic flaw growth relation, e.g., Eq. (A-1), and on residual stresses. We shall consider only the former case here. There is a limited amount of evidence from adhesive crack growth tests[6] and other fracture studies of polymers[15] that the exponent in Eq. (A-1) does not change significantly over wide temperature ranges; but c changes appreciably with temperature. Thus, we may account for the effect of different constant temperatures or transient temperatures on

on fatigue life by simply introducing the relevant temperature dependence of C in Eq. (A-16).

It should be recalled that C, which is defined through Eq. (A-11), is the ratio of the current value of the crack growth coefficient to its "initial" value. With temperature changes, the initial value of the coefficient, c_{oi}, should be interpreted as the value existing at some preselected reference temperature, T_R. Then, making the reasonable assumption that the temperature dependence of the dominant crack growth rate is the same for all specimens, we conclude that Eq. (A-16) is applicable.

In general, C may change due to temperature as well as other parameters such as global strain level and microscopic fatigue damage of the adhesive. If, however, only temperature changes are important, then C = 1 at $T = T_R$.

APPENDIX B

EFFECT OF STRAIN ENERGY IN THE ADHESIVE ON CRACK GROWTH

In Section 4.3 and Appendix A the contribution of the adhesive to energy release rate is neglected. Here we estimate this contribution for the thin adhesive layer and show that it can have a large effect on crack growth.

Consider the butt joint in Figure B-1, in which the applied stress is σ_∞. The crack need not be centered between the adherends. An approximate formula for energy release rate will be derived by adding the energy for the two limiting cases of (i) rigid adherends and (ii) adhesive with zero thickness (H = 0).

For rigid adherends and a thin adhesive layer, we may assume that the only strain in the adhesive (except near the crack tips and near the free surface) is the thickness strain, ε_z, and that ε_z is independent of Z. Let the normal stress-strain equation be written as

$$\sigma_z = E_H \varepsilon_z \tag{B-1}$$

Then, the strain energy density is

$$W_H = \frac{E_H}{z} \varepsilon_z^2 \tag{B-2}$$

and the total strain energy in the adhesive is

$$W_H = \frac{1}{2} \int_{A_u} H E_H \varepsilon_z^2 dA + W_c \tag{B-3}$$

where A_u is the uncracked, cross-sectional area and W_c is the strain energy correction for crack tip and free-surface effects. The strain energy change when an amount of crack surface $dA_c = 2\pi a da$ is formed with fixed adherends is simply equal to the strain energy contained in a volume HdA_c if the change in W_c is negligible; this latter condition will be valid in most cases if the advancing crack tip is not within a few adhesive thicknesses of other cracks or of the free surface. Hence,

$$\frac{dW_H}{dA_c} = - \frac{H E_H}{2} \varepsilon_z^2 \tag{B-4}$$

As long as the crack tip is at least several thicknesses, H, away from the free surface (r = R), we may write

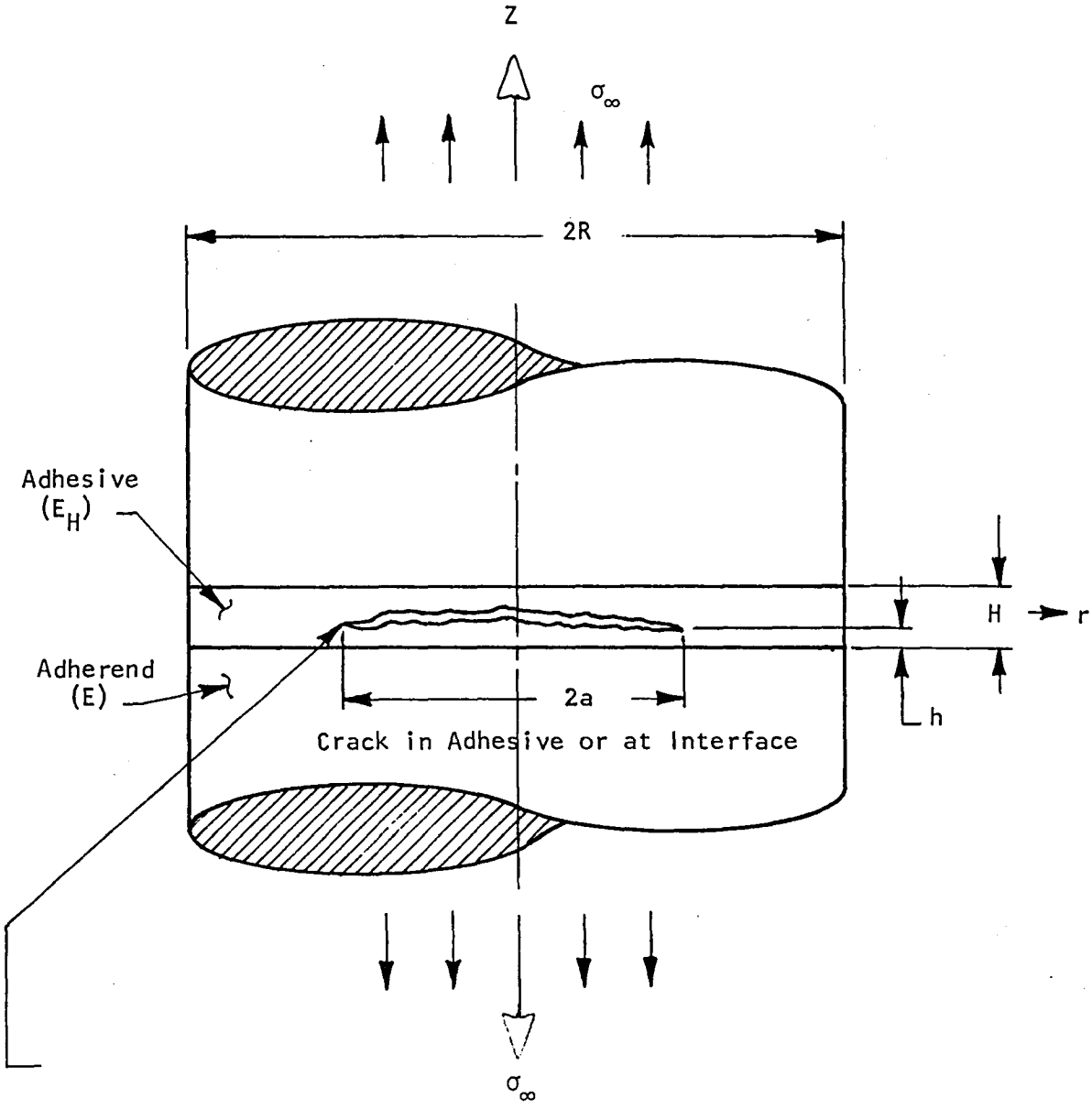

FIGURE B-1. CIRCULAR BUTT JOINT WITH PENNY-SHAPED CRACK

$$\varepsilon_z = \frac{\sigma_z}{E_H} = \frac{\sigma_\infty R^2}{(R^2-a^2)E_H} \tag{B-5}$$

Thus, Eqs. (B-4) and (B-5) yield the strain energy release rate due to the adhesive,

$$G_H = \frac{H\,\sigma_\infty^{\,2}}{2E_H\left(1-\frac{a^2}{R^2}\right)^2} \tag{B-6}$$

As the second limiting case, corresponding to H = 0, we start with the stress intensity factor for a penny-shaped crack in an infinite body,

$$K_I^{(P)} = \frac{2}{\sqrt{\pi}}\sqrt{a}\;\sigma_\infty \tag{B-7}$$

The energy release rate is derived from the standard formula,[22]

$$G_p = \frac{1-\nu^2}{E}\left(K_I^{(P)}\right)^2 \tag{B-8}$$

where E and ν are the Young's modulus and Poisson's ratio of the adherend. Thus,

$$G_p = \frac{4}{\pi}\frac{(1-\nu^2)a}{E}\sigma_\infty^{\,2} \tag{B-9}$$

The effect of the reduction in loaded area on this energy is not as significant as that in Eq. (B-6) except for cracks which are close to the free surface[23]; therefore, this effect will be neglected.

The total energy release rate is assumed to be the sum of Eqs. (B-6) and (B-9),

$$G = \frac{H\sigma_\infty^{\,2}}{2E_H\left(1-\frac{a^2}{R^2}\right)^2} + \frac{4(1-\nu^2)a\sigma_\infty^{\,2}}{\pi E} \tag{B-10}$$

An "effective" stress intensity factor is now introduced through the definition

$$K_I \equiv (EG)^{\frac{1}{2}} \tag{B-11}$$

This is the factor which is used in representing data from the CDCB test, and therefore should be used in predicting crack growth and failure of a butt joint.

Thus,

$$K_I = (a_H+a)^{\frac{1}{2}} \left[\frac{4}{\pi}(1-\nu^2)\right]^{\frac{1}{2}} \sigma_\infty \tag{B-12}$$

where

$$a_H = \frac{\pi}{8} \frac{E\ H}{E_H(1-\nu^2)\left(1-\frac{a^2}{R^2}\right)^2} \tag{B-13}$$

Eq. (B-12) shows that the stress intensity factor is the same as that in a joint with negligible adhesive strain energy ($H \simeq 0$) if the crack is of radius a_H+a instead of a. If the correction for area change is neglected the increase in crack radius, a_H, is constant. For example, with a soft adhesive

$$E_H = \frac{(1-\nu_a)\ E_a}{(1+\nu_a)(1-2\nu_a)} \tag{B-14}$$

where E_a and ν_a are the Young's modulus and Poisson's ratio of the adhesive. From Table 3-1, E_a = 1.12GPa(162 KSI), using a typical value of $\nu_a = 0.35$ for plastics, we find

$$E_H = 1.79 \text{ GPa}(260 \text{ KSI}) \tag{B-15}$$

For aluminum, E = 71.0 GPa (10.6×10^3 KSI) and $\nu = 0.33$. Therefore, if H = .025 cm(0.01 inches), a very significant correction is obtained,

$$a_H \simeq .762 \text{ cm}(0.30 \text{ inches}) \tag{B-16}$$

In contrast to this result, the effect of adhesive thickness in the CDCB specimens is found to be negligible.[24]

Finally, it should be noted that Eq. (B-10) and the associated stress intensity factor for the penny-shaped crack have been compared with the numerical predictions in Reference 25; also, we have made similar comparisons for analogous plane-strain problems.[26] For a realistic range of properties good agreement was found. (However, it is believed that there is an error at H = 0 in References 25 and 26 because an incorrect limit was taken to evaluate a certain constant. Namely, it was assumed that crack opening displacement remains continuous as $H \to 0$; however, it is the energy release rate which has this continuity property. After making this correction, good agreement was achieved for a realistic range of properties.)

DO NOT REMOVE SLIP FROM MATERIAL

Delete your name from this slip when returning material to the library.

NAME	DATE	MS

NASA Langley (Rev. Dec. 1991) RIAD N-75